



***Università degli Studi di Salerno***

Dipartimento di Ingegneria dell'Informazione ed Elettrica e  
Matematica Applicata

Dottorato di Ricerca in Ingegneria dell'Informazione  
XIV Ciclo – Nuova Serie

TESI DI DOTTORATO

# **Degradation of OLEDs devices: study methods and solutions**

CANDIDATO: **ELENA SANTORO**

TUTOR: **PROF. ALFREDO RUBINO**

TUTOR ENEA: **DOTT. MARIA GRAZIA MAGLIONE**

TUTOR ENEA: **DOTT. ING. GIULIANO SICO**

COORDINATORE: **PROF. MAURIZIO LONGO**

Anno Accademico 2014 – 2015

*In loving memory of  
my cousin Chiara*

*The greatest enemy of knowledge is not ignorance,  
it is the illusion of knowledge.*  
**Stephen Hawking**

## Acknowledgements

I would like to extend my acknowledgements to the many people that in different ways have generously contributed to the work presented in this thesis.

I am sincerely grateful to my supervisor, Prof. Alfredo Rubino, for everything he taught me in these years, always encouraging and helping me to do better. This thesis work would not have been possible without him.

I would like to thank Ph.D. School coordinator, Prof. Maurizio Longo, for his support during Doctoral School in Information Engineering.

I remain grateful to Dr. Eng. Carla Minarini, who welcomed me at the ENEA institute in Portici, allowing me to use their working equipment, and supporting me during my permanence at there.

I am profoundly thankful to my ENEA supervisor, Dr. Maria Grazia Maglione who first introduced me to Organic Devices Encapsulation giving me the opportunity to work on this topic and allowing me to learn from all her experience.

I am indebted to Eng. Paolo Tassini for his guidance, for the patience and good advices.

My sincerest thanks go to Dr. Eng. Giuliano Sico, from ENEA, for the long time spent with me, sharing his knowledge, and for being so dedicated to his role as my secondary supervisor. I'm very thankful for his help with permeation topics, for the long hours in the clean room, talking about scientific subjects and lots of other things.

I owe my deepest gratitude to my friend and PhD colleague, Eng. Maria Rosa Fiorillo, for her never-ending friendship, Eng. Salvatore Aprano for his help and all the deposition processes, Dr. Tania Prontera for her friendship, for all the photolithography processes and for the help in experimental moment and Dr. Luca Iannuzzi for the informatics support.

I would like to show my gratitude to all the people met at the institute ENEA Portici who offered me their friendship, helping me and

sharing with me their time and particularly to Martina, Claudia, Maria Laura: it has been a pleasure to meet you all.

I feel thankful towards colleagues and students met during my experience.

And now I want to thank people who have been by my side from the beginning.

My immensurable gratitude goes to people who are always there for me Alessandra, Maria Luisa, Luca and Maria again your friendship has an incommensurable value.

I also would like to thank my volleyball teammates for their constant support when, year after year, I was studying in any possible moment before and after our practices, and even on the road for our matches!

The greatest thank goes to my parents, for their unconditioned love and support.

Special thanks to all my wonderful family and to my family in law: we have been one big family from the first beginning.

Finally, I want to thank my husband Sergio. The love he shows me every single moment in good and bad days makes me face difficulties and failures. He always trusted me and my talent even when I didn't have faith in myself.

There are no words to describe how much I love him.

**Thank you all**

**Love you**

*Elena*

# Table of Contents

Introduction .....	1
1 Organic Electronics .....	6
1.1 Organic semiconductors .....	6
1.1.1 Carbon atom bonds.....	7
1.1.2 Conjugated system .....	9
1.2 Charge Transport .....	10
1.3 Electrical Conduction .....	13
1.3.1 Injection limited conduction.....	14
1.3.2 Space Charge limited conduction.....	16
1.4 Basic Organic Electronics Devices.....	17
1.4.1 Organic Thin Field Transistor .....	17
1.4.2 Organic Solar Cells .....	18
1.4.3 Organic Light Emitting Diode (OLED) .....	20
1.5 Degradation of OLED Devices.....	24
2 Principle of permeation and barrier technology .....	27
2.1. Principle of permeation .....	27
2.1.1 Adsorption and desorption .....	28
2.1.2 Diffusion.....	29
2.1.3 Permeation.....	30
2.2 Permeation Measurement Techniques.....	33
2.2.1 Coulometric Devices .....	34
2.2.2 Mass Spectrometry .....	35
2.2.3 Laser absorption .....	36
2.2.4 Calcium Corrosion Tests .....	36
2.3 Barrier Requirements.....	38
2.4 Encapsulation solutions .....	39
2.4.1 Glass to glass approach .....	40

---

2.4.2	Lamination of film barrier .....	41
2.4.3	Thin Film Encapsulation .....	42
2.4.4	Multilayer approach.....	48
3	Development of an Electrical Calcium Corrosion Test measurement system.....	51
3.1	Electrical Calcium test choice.....	51
3.2	Layout design.....	52
3.3	Measurement setup .....	55
3.4	Sample realization.....	56
3.5	Evaluation of measurement curves and WVTR calculation	58
3.6	Limitation and future perspective of Electrical Calcium Test	60
4	Development of a glass to glass encapsulation system .....	62
4.1	Layout choice.....	62
4.2	Encapsulation process parameters optimization .....	63
4.3	Encapsulation characterization through Electrical Calcium Test	66
4.3.1	Calcium Test results at ambient condition .....	68
4.3.2	Calcium Test results for various conditioning.....	70
4.4	Validation of the encapsulation system through device degradation in accelerated atmosphere.....	70
5	Development of a flexible barrier layer encapsulation system ..	75
5.1	Thin Film Encapsulation choice .....	75
5.2	Developing and optimizing of single thin inorganic Al <sub>2</sub> O <sub>3</sub> layer for multilayer barrier structure .....	76
5.3	Developing and optimizing of organic intralayer for multilayer barrier structure .....	80
5.4	Making multilayer inorganic-organic barrier structure on flexible PEN substrate .....	83
6	Intrinsic degradation study .....	87

<i>Table of Contents</i>	iii
6.1 New methodology for intrinsic degradation study .....	87
6.2 Case study: blue OLED devices .....	89
7 Conclusion and future perspective .....	96
7.1 Conclusion .....	96
7.2 Future perspective.....	98
8 Table of Figures .....	100
9 Bibliography.....	105







## Introduction

The fast technological evolution of our world requests the necessity to make this development sustainable. In order to achieve this goal more relevance has been given to the energy consumption and environmental impact of the modern society consumerism.

These considerations point out the need to increase the effort in research of unconventional materials, new concept and system architecture for devices that could help to overcome these challenges.

Nanotechnologies offer the best chance for this innovation and particularly organic electronics has been encouraged thanks to new attractive properties and promising applications.



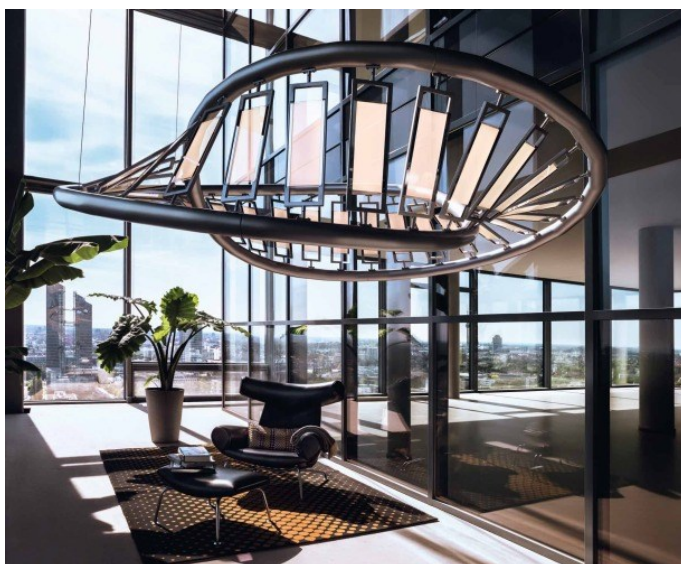
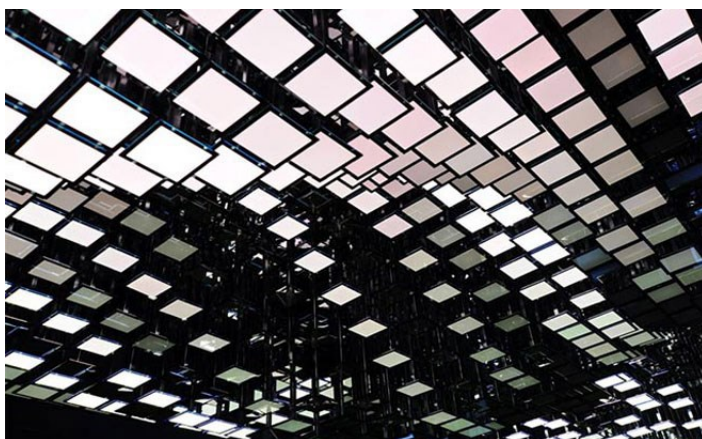
Organic materials could be processed in thin film accommodating the issue of preservation of manufacturing energy usage despite from bulky and costly processes of inorganic industries. Fabrication techniques, including spin or spray coating, ink-jet or roll-to-roll printing, can be applied at low-temperature and over large area substrates. This is promising to maximize production throughput and to reduce costs. Also many other advances have been reached in the electronic applications of organic materials such as the spread of light-

weight, transparent, flexible and disposable devices. Particularly, in recent years, OLEDs (Organic Light Emitting Diode) have been successful commercialized both for display applications and light source. OLED-based displays are nowadays commercialized both for high performances cell displays and TVs, becoming the major competitors of other well established technologies, like LCD or LED.



In imaging application, very often Active Matrix approach is used to supply the display. In recent years the use of another Organic Electronics device, Organic TFT (OTFT), has been exploited as Active Matrix driver with encouraging results.

In the last years also OLED-based light source have been introduced on the market. OLED panel technology allows overcoming some of the more critical issues of the preceding technologies such as very low energy conversion, as for incandescence source light, lack of good colors and the use toxic elements as for fluorescent tube and costly manufacturing processes and point light source as for the more recent LED technology.



Despite all these amazing results, important drawbacks still remain in the field of organic electronic devices. Low charge carrier mobilities or still expensive manufacturing cost, but the more critical is extreme sensitivity to ambient conditions, temperature, light, and particularly oxygen and moisture, which could degrade their optical and electrical characteristics.

This work of thesis sets in this scenario and the aim of this research is the study of degradation phenomena through methodology that leads

to the identification of the different mechanisms of degradation involved, responsible of device short life time.

The present work has been developed focusing the attention on the various degradation mechanisms in OLED and the possibility to use their nature to develop innovative analysis methods. For this purpose has been exploited both extrinsic and intrinsic degradation. Critical issues in this field are the complexity of the involved phenomena and the relatively recent interest of the scientific community in the intrinsic degradation topic.

Through the work organic devices and Calcium test sample have been fabricated and a series of experiments have been carried out to investigate their performance. All devices have been fully processed in the cleanroom (class 100) located at ENEA Portici.

In the organization of the thesis work, after a brief presentation of the main features of organic electronics in Chapter 1, an overview of the basic principles of permeation and typical encapsulation solutions are presented in Chapter 2. In particular, specific attention has been paid on barrier requirements and solutions presented to protect the devices. These solutions, besides being the way to control extrinsic degradation, are also used to isolate other degradation components becoming a tool for studying the intrinsic degradation in organic devices. In the Chapter has been also pointed out the importance to evaluate the barrier characteristic in terms of WVTR and here has been presented some solution to evaluate ultra-high barrier permeation. The study has been then centered on the design and development of a Calcium corrosion test for the barrier evaluation described in detail in Chapter 3. It has been investigated all the aspect of layout and setup to achieve a higher sensitivity level. This measurement method has been employed for the design and optimization of both a glass to glass and Thin Film Encapsulation barrier permeation system respectively presented in Chapter 4 and Chapter 5. In the first case (glass to glass) the developed encapsulated system has been used in an effective way to estimate lifetime of a simple OLED structure and validate the system performances.

Afterwards, the investigations have been focused on intrinsic degradation process. For this purpose the glass to glass encapsulation system has been also used to neglect external agents within the development of an innovative method based on accelerated

environmental aging conditions for the study of intrinsic degradation phenomena components. Thus an innovative methodology to study this issue has been proposed and tested on a case study in Chapter 6.

## Chapter 1

# 1 Organic Electronics

In nature we can find a huge variety of materials that have in common they contain carbon known as *organic materials*. Since some of these organic materials exhibit semiconducting properties they can be employed to fabricate electronic devices showing a multiplicity of desirable features made them appealing from both industrial and scientific point of view.

Simple production processes, materials availability and versatility, mechanical flexibility, innovative devices and large area applications combined with cost-effective, reduced power consumption [1] are just a few aspects that made Organic Electronics a research priority of many industries, universities and research institutes worldwide. In this Chapter the basic properties of organic compounds will be described, focusing attention to the semiconducting behavior. Then some organic devices will be shortly presented.

## 1.1 Organic semiconductors

Almost all carbon-based compounds are classified as organic materials except for few carbon-containing materials such as carbide, diamond, or  $C_{60}$ . They can occur in a variety of molecular structures and, depending on their molecular weight, they are distinguished in small molecules or polymers. Some of those organic materials exhibit semiconducting properties and this motivates their large diffusion. The difference between semiconductors and electrical insulators is due to the size of the energy gap electrons must overcome. In contrast to inorganic semiconductor, organic materials are rarely crystalline and

the overlap between the orbitals of two molecules is small. Thus the energy levels of the molecules do not split up to whole bands, and the electron mobility, which requires hopping of electrons from one molecule to the next, is low. Due to their low conductivity, organic semiconductors have to be deposited in very thin layers (orders of magnitude ranging from 1 to 500 nm) to keep the driving voltage of the organic devices in the range of some volts. The deposition processes of these thin layers depend on the size of their molecules.

Small molecules are light enough to be thermally evaporated without being decomposed and the desired geometry can be obtained via shadow masks. On the contrary, polymers are larger molecule, hence the van-der-Waals interaction between their single molecules is larger than for small molecules and they decompose below their evaporation temperature. Consequently, those polymers are spin-coated or printed onto surfaces from solutions, and the corresponding solvents are then removed via a curing process. Printing is an excellent process for large-scale applications, but the process is limited to a few layers, since the solvent of further layers should not wash away the layers underneath.

### 1.1.1 Carbon atom bonds

In organic materials, the semiconducting property originates from carbon atoms bonds. Let us consider the electronic configuration of an isolated atom of Carbon:  $2s^2 2p^2$ . When carbon atoms come together, the s orbitals and three p-orbitals mix themselves forming equivalent states leading to concept of "hybridization". If Carbon orbitals form four equal states, tetrahedrally arranged, we are talking about  $sp^3$  hybridization [2]. Molecular bonds arising from  $sp^3$  and s orbitals (e. g. Methane) are called  $\sigma$ -bonds. They have large binding energies because electrons are strongly localized.

Another possible Carbon configuration is that obtained in the so called  $sp^2$  hybridization. In this case only two of 2p states mix with 2s, obtaining three  $sp^2$  orbitals plus a not hybridized p one. They can form three planar  $\sigma$  bonds while the remaining not hybridized p-orbitals form  $\pi$  bonds. Here electrons are more delocalized (over several atomic units) and binding energies are low, making the  $\pi$  bond weaker than the  $\sigma$  one.

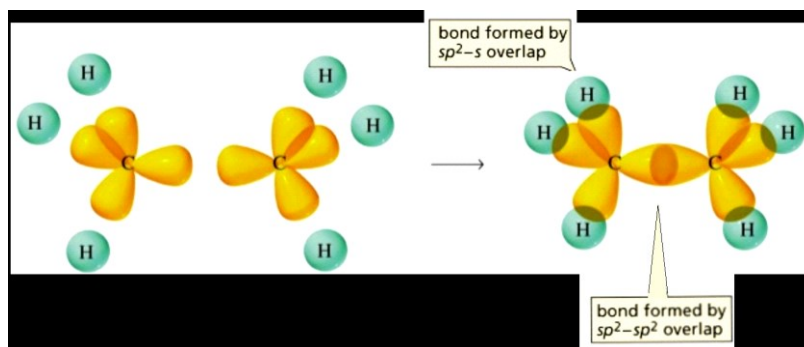


**Figure 1.1** - Carbon  $sp^3$  hybridization made of three  $2p$  orbitals mixed with  $2s$  orbital forming four hybridized  $sp^3$  states in tetrahedral spatial configuration. Two Carbon  $sp^3$  atoms forming  $\sigma$  bond.

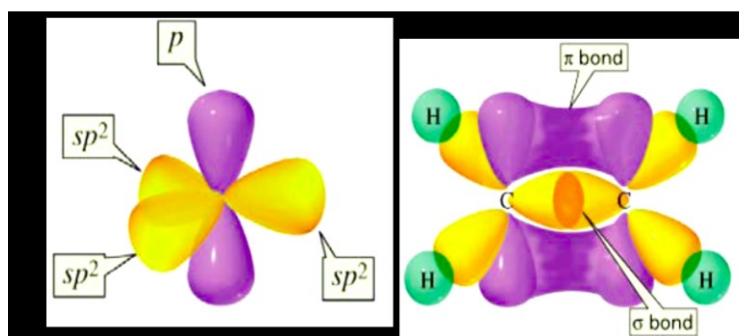


**Figure 1.2** - Carbon  $sp^2$  hybridization made of two  $2p$  orbitals mixed with  $2s$  orbital forming three hybridized  $sp^2$  states plus one un-hybridized  $2p$  orbital. Two Carbon  $sp^2$  atoms forming double  $\sigma$  and  $\pi$  bond.

Hence two neighboring  $sp^2$  carbon atom share a double bond, a  $\sigma$  bond and a  $\pi$ -bond. Orbitals' overlap leads to two different electron wave functions: a bonding wave function and an anti-bonding wave function. In the case of  $\sigma$  bond the large orbital overlap leads to a high energy splitting between bonding and anti-bonding states, i.e. a large energy gap. So became clear that the semiconducting property cannot stem from  $\sigma$  bond because of the large energy gap between bonding and antibonding states, but the electronic states of organic molecules are generated from the  $p$  orbitals of carbon atoms through  $sp^2$  hybridized orbital. The  $p$  orbitals are oriented perpendicular to the plane of the  $sp^2$  hybrid orbitals. Hence, the  $p$  orbitals of two neighboring carbon atoms exhibit only a very slight overlap causing

only a slight energy splitting between the bonding ( $\pi$ ) and anti-bonding ( $\pi^*$ ) electron wave functions. Consequently, the related electrons are less localized between or outside the atoms than in the strong  $\sigma$  bond. Such an overlap of p orbitals is called conjugation.

### 1.1.2 Conjugated system

Organic molecules consist of many carbon atoms, (i.e. molecules formed by Carbon rings or chains) that alternating single and double carbon bounds, give rise to the so called conjugated system (or  $\pi$  system) where the  $\pi$  electrons are weakly bound and can be delocalized inside a molecule. Delocalization due to  $\pi$  orbitals is responsible for electrical conductivity. In complex conjugated systems a large number of atomic orbitals overlap, resulting in one group of energy states above and one group of energy states below the energy gap, giving birth to quasi-continuum energy bands made by splitted energy levels.

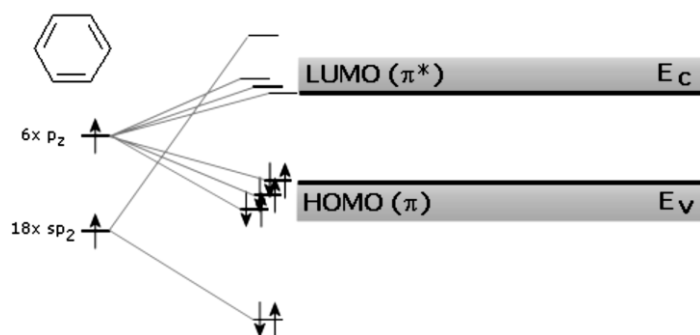


**Figure 1.3** - Band structure of a Carbon ring. It can be seen that an energy gap occurs from  $\pi$  and  $\pi^*$  bonds, while bands formed by  $\sigma$  and  $\sigma^*$  states lie at lower and higher energies (respectively).

More precisely the slight overlapping of p orbitals defines the analogous to the valence band and conduction band of an inorganic semiconductor. In detail, the highest  $\pi$  bonding states, that is occupied by electrons and belongs to the lowest group of states, is called HOMO (Highest Occupied Molecular Orbital) and is the lower limit of the gap while the lowest  $\pi$  antibonding state that is unoccupied and belongs to the higher group of energy states is called LUMO (Lowest Unoccupied Molecular Orbital) and represents the upper limit of the

gap. The larger the connected system of  $\pi$  bonds is, the smaller the energy gap becomes. Consequently, modifying the chemical structure changes the energy gap of these molecules; this modification can therefore be used to adjust their emission and absorption behavior. Despite from the behavior described so far, a fundamental and essential difference of conjugated systems from inorganic semiconductor is that the latter have a very crystalline structure made up from single atoms.

Organic materials which exhibit semiconducting properties possess an intermediate structural unit: the molecule. Strong covalent bonds dominate within the molecule, but between molecules, weak van-der-Waals-bonds dominate. The low interaction forces between the molecules have many consequences for the solid but the most important concern the charge transport mechanisms. While in Silicon charges are almost “free” to move over the material, in organic semiconductors electrons and holes have to “hop” from a molecule to another (hopping conduction).

## 1.2 Charge Transport

The fundamental mechanisms of electron and hole transport in organic solids are not fully understood. Only in the very special case of high material purity, low temperature and high crystallinity, organic materials can exhibit band-like transport behavior similar to that of classic semiconductor. More often organic semiconductors show a disordered structure, so the charge carriers move through an intermolecular process, hopping between adjacent molecules.

Moreover, they can be localized by defects, disorder or potential wells caused by the polarization. If the lattice is irregular or the carrier becomes localized on a defect site, the lattice vibrations are essential to let the carrier move from one site to another. This is an activated process and the mobility increases with increasing temperature. Obviously, the latter is a less efficient mechanism respect to the former.

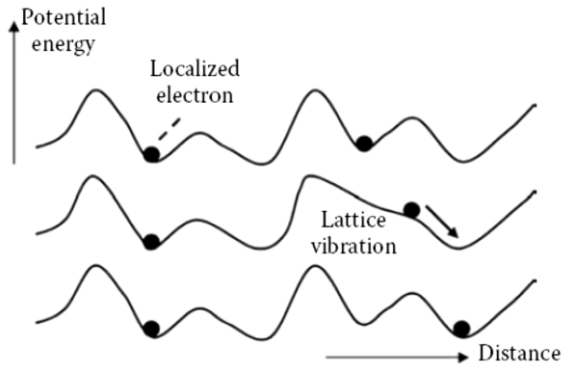


**Figure 1.4** - Hopping transport mechanism

Independently from the specific mechanism of electron movement, conduction based on electron movement can be described by the following formulas:

$$J = \sigma \vec{E} \quad (\text{macroscopic description}) \quad (1.1)$$

$$J = -qn\mu_e \vec{E} \quad (\text{microscopic description}), \quad (1.2)$$

where  $J$  is the current density,  $\sigma$  is the conductivity,  $q$  is the elementary charge,  $n_e$  electron density,  $\mu_e$  electron mobility defined as:

$$\mu_e = \frac{v_d}{E} \quad (1.3)$$

and  $v_d$  is the drift velocity of electrons.

In the first expressions, the macroscopic conductivity refers to a density of electrons that move, on the micro-scale, with the drift velocity. The mechanism of electron movement is hidden within the electron mobility  $\mu_e$  that represents the relation (ratio) between applied field strength and drift velocity.

Focusing on the most common case of disordered organic materials, it is here illustrated two models applied to describe the hopping conduction mechanism: the Nearest Neighbor Hopping (NNH) and the Variable Range Hopping (VRH). In the former, an electrical charge

“jumps” from a spatial localized energy level to the nearest neighbor (Figure 1.5. a), while in the latter the charge can jump several levels away from the original one, i.e. variable range (Figure 1.5. b)

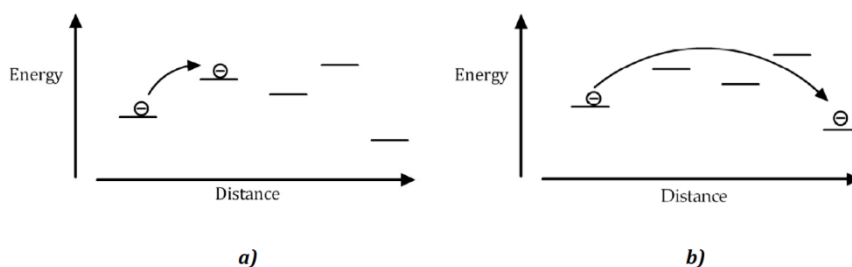


**Figure 1.5** - Hopping conduction: a) nearest neighbor hopping, b) variable range hopping.

The transition probability from one energy level to another is expressed as the product of some terms, taking into account:

- wavefunctions overlapping between states: this term has an  $\exp(-\alpha R)$  dependence, where  $\alpha^{-1}$  is the wave function localization length and  $R$  is the distance between initial and final levels;
- Phonons availability: if the initial and final states have energy separation of  $W$ , energy conservation rules require a second particle bridging this gap, in order to enable the charge hop. This mechanism is generally fulfilled through molecules vibration, i.e. phonons. The term dependence is  $\exp(-W/k_B T)$ , where  $k_B$  is Boltzmann constant and  $T$  is temperature;

The probability per unit time of a charge jumping between two localized states is therefore proportional to:

$$p \sim \exp(-Q) \quad (1.4)$$

$$Q = \left( \alpha R + \frac{W}{k_B T} \right) \quad (1.5)$$

When  $W$  is smaller than  $k_B T$ , the  $\alpha R$  term dominates, leading to a NNH mechanism;  $Q$  is minimized for minimum  $R$ , when the final level is the nearest one. On the other hand, when  $T$  is low and phonons

energy and number are small;  $W/k_B T$  cannot be neglected with respect to  $\alpha R$ . In this situation, balancing energy and distance, a distant level could possess a smaller  $Q$  than the nearest neighbor and a VRH regime occur.

Hypothesizing a casual diffusive mechanism as driving force of electron motion electrical conductivity ( $\sigma$ ) in hopping regime can be calculated as follow:

$$\sigma = qn\mu \quad (1.6)$$

$$\mu = \frac{qD}{k_B T} \quad (1.7)$$

$$D = \frac{1}{6} p R^2 \quad (1.8)$$

Here,  $q$  is electron charge,  $n$  is electron density and  $\mu$  is charge mobility, determined by Einstein relation.  $D$  is diffusion coefficient, in which hopping probability is taken into account according to NNH mechanism. On the contrary, in the case of VRH regime, conductivity has the characteristic temperature dependence expression

$$\sigma = \sigma_0 \exp \left[ \left( -\frac{T_0}{T} \right)^{\frac{1}{4}} \right] \quad (1.9)$$

where  $T_0$  and  $\sigma_0$  are constant given by model parameters ( $R$ ,  $\alpha$ , etc.).

### 1.3 Electrical Conduction

In order to understand the electrical behavior of organic devices, electrical conduction could be represented using a huge variety of current-voltage models.

These models essentially belong to two families of phenomena that limit the conduction: *injection limited conduction* and *bulk limited conduction*.

### 1.3.1 Injection limited conduction

When current is determined by injection properties over a potential barrier, we can use the following models [3]:

Thermionic emission Charge carriers are driven by diffusion over a potential barrier. Here,  $A^*$  is Richardson effective constant,  $T$  is temperature,  $k$  is Boltzmann constant,  $\Phi_e$  is potential barrier height,  $n$  is ideality factor,  $J$  is current density and  $V$  is applied voltage

$$J_{TE} = A^*T^2 \exp\left(-\frac{\Phi_e}{kT}\right) \left[\left(\frac{qV}{nkT}\right) - 1\right] \quad (1.10)$$

Schottky-Richardson thermionic emission The basic thermionic model is modified for field-assisted emission over the potential barrier. Here,  $A^*$  is Richardson effective constant,  $T$  is temperature,  $k$  in Boltzmann constant,  $\Phi_e$  is barrier height,  $d$  is device thickness,  $q$  is electron charge,  $\epsilon$  is electrical permittivity of material,  $J$  is current density and  $V$  is applied voltage. A uniform electric field ( $E$ ) distribution is considered, i.e.  $E = V/d$

$$J_{SR} = A^*T^2 \exp\left(-\frac{\phi_B}{kT}\right) \quad (1.11)$$

$$\phi_B = \phi_e - \sqrt{\frac{qV}{4\pi\epsilon x_m}} \quad (1.12)$$

$$\Delta\phi = \sqrt{\frac{qV}{4\pi\epsilon x_m}} \quad (1.13)$$



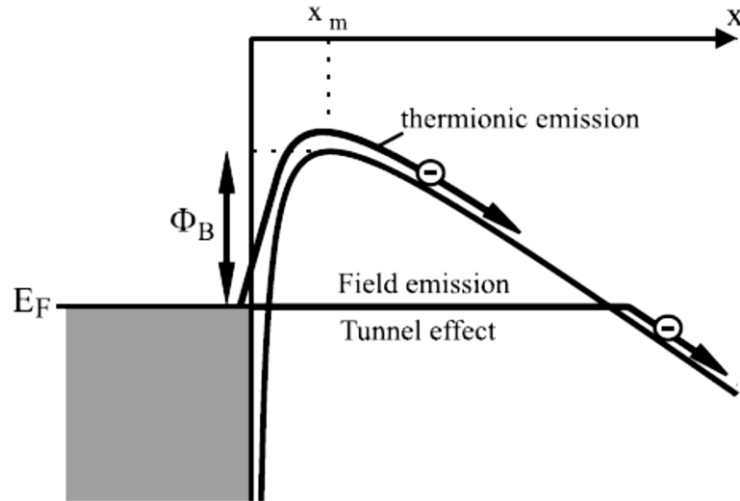


Figure 1.7 - Schematic of barrier level for Fowler-Nordheim tunneling

### 1.3.2 Space Charge limited conduction

When current is determined from material bulk conduction properties, we can take into account the following models:

Nearest Neighbor Hopping conduction (NNH) Here  $J_0$  is a constant depending on material properties,  $R$  is NNH distance,  $d$  is device thickness,  $V_T$  is thermal voltage,  $J$  is current density and  $V$  is applied voltage. A uniform electric field ( $E$ ) distribution is considered, i.e.  $E=V/d$ .

$$J_{NNH} = J_0 \sinh\left(\frac{RV}{dV_T}\right) \quad (1.15)$$

Space Charge Limited Conduction (SCLC) This originates when in a material is injected more charge than that thermally generated. Here,  $\mu$  is mobility (considered constant with electric field),  $d$  is device thickness,  $\epsilon$  is electrical permittivity of material,  $J$  is current density and  $V$  is applied voltage

$$J = \frac{9}{8} \varepsilon \mu \frac{V^2}{d^3} \quad (1.16)$$

This expression is valid in the case of a Trap Free material and the model is known as TF-SCLC. Typically an organic material is not trap free but they are present and limit the current. The carriers are captured occasionally by shallow traps and are remitted back thermally: this effect is significant as the level of trap is close to the conduction band. On the other hand the deep traps, however, are located below the Fermi level and for this reason they tend to be occupied and to localize the charges. When all the traps are filled, the current is no more under traps influence, and has a trend formally identical to that in absence of trap states. Modifying the expression to include the effect of the traps in SCLC model it is sufficient to replace the mobility  $\mu$  with an effective mobility  $\mu_{\text{eff}}$ .

## 1.4 Basic Organic Electronics Devices

In spite of organic materials low conductivities and lower transport performances, through the past years, almost all typology of inorganic devices have been realized employing organic semiconductor obtaining very interesting results.

### 1.4.1 Organic Thin Field Transistor

Organic Thin Field Transistors (OTFT) electrical behavior is conspicuously similar to classic FETs. They are three terminal devices where current between two electrodes, i.e. source and drain, connected with the semiconductor, is controlled by modulation of channel conductivity, performed by another voltage applied to an insulated gate electrode.

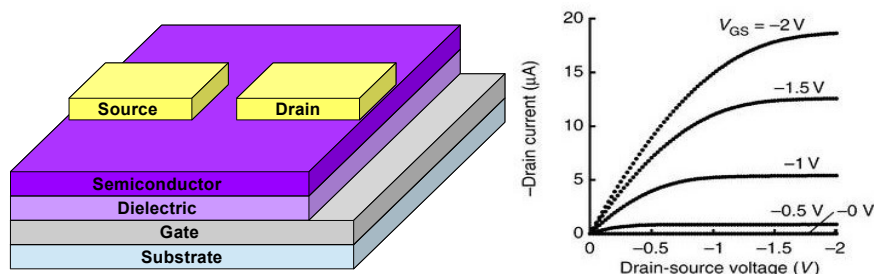


**Figure 1.8** - OTFT in top contact configuration and typical OTFT curves

OTFTs are “normally-on” devices; i.e. without any voltage applied to the gate there is still a current flow between source and drain. Applying a gate voltage of proper bias charges move away from the channel, forming a depletion region that stops the source drain current. Different configurations of OTFTs exist, depending on the deposition sequence of the different layer and the position of electrode.

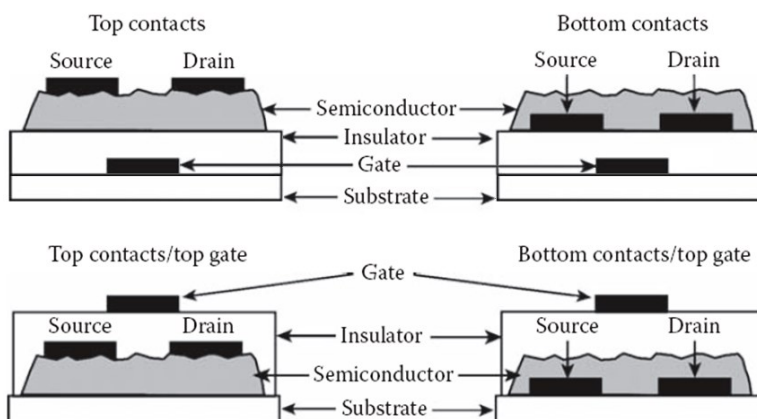


**Figure 1.9** - Four possible configurations for an OTFT.

OTFTs have been successfully used as drivers in AM displays and their field of application is continuously and rapidly enlarging.

## 1.4.2 Organic Solar Cells

Organic devices expanded in the field of renewable energy, with Organic Photovoltaic (OPV). Also in this case, device basic principles

are essentially similar to their inorganic counterparts: light enters a semiconducting material and photons with energies above the energy gap are absorbed and thereby generate electron-hole pairs (excitons). These excitons have to split up to generate a free electron and a free hole. Thus, if the organic material is to serve as an electron donor in OPVs, a second material is required as an electron acceptor to ensure a built-in internal field at the interface to break up any excitons that diffuse there into free carriers, both of which are conducted to opposite electrodes. This D-A interface concept is analogous, in terms of charge transport, to a P-N junction in an inorganic semiconductor [4].

The electrical potential difference between electrons and holes at these electrodes is used as an electrical power source when the electrodes are connected over an external circuit. Of course only photons with energies larger than the energy gap excite electrons. On the other hand, photons with energies below the energy gap cannot create excitons. For those photons, the semiconductor is transparent.

Hence, single solar (i.e. single junction) cells cannot convert all of the light energy to electrical energy [5]. The problem can be reduced by using tandem cells, wherein a cell with a large energy gap at the front efficiently extracts the energy from high-energy photons, and a cell with a small energy gap behind the first cell efficiently extracts the energy from the transmitted low-energy photons.

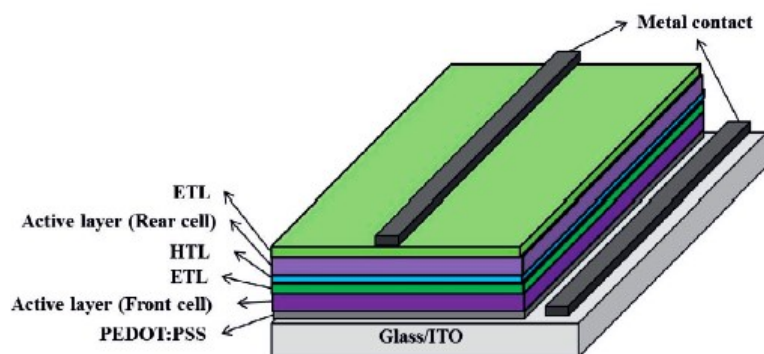


**Figure 1.10** - Schematic of device structures of conventional multi-junction tandem cells

At present, most used single cell configurations are conventional and inverted device structures based on indium tin oxide (ITO) electrode .

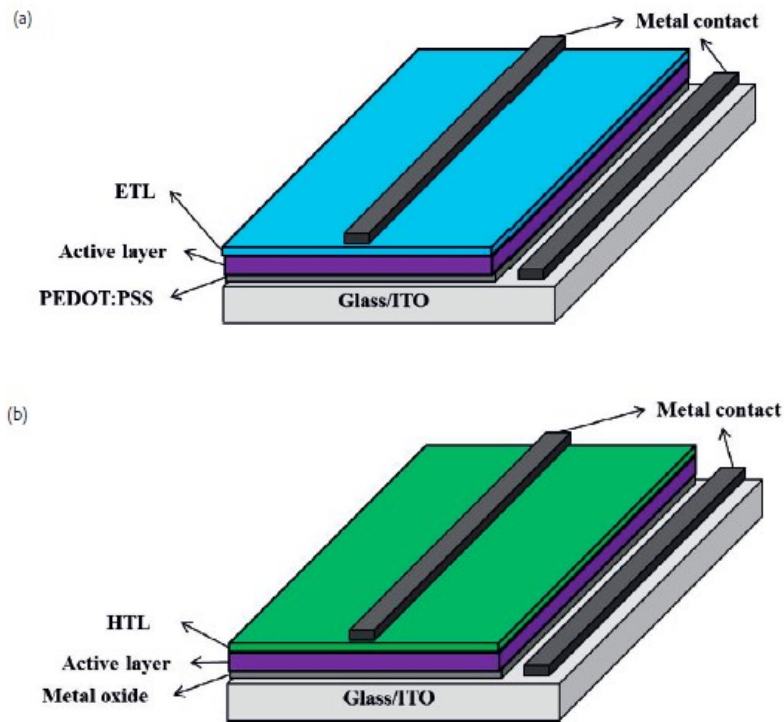


**Figure 1.11** - Schematic of device structures of (a) conventional single-junction cell, (b) inverted single-junction cell [4]

OPV efficiencies have recently reached up to 12% and following efficiency growth trends, organic cells improvements have been wider than the amorphous Silicon, so that OPV could replace that technology in coming years.

### 1.4.3 Organic Light Emitting Diode (OLED)

Organic Light-Emitting Diodes (OLEDs) represent perhaps the most promising application of organic electronic. OLEDs become more and

more popular thanks to their application into high performances displays, but are now used in lighting application due to some obvious benefits. First OLEDs emit light from an area, more pleasant to the eye than point sources of light, and then their color is easily tunable within a wide range via the choice of emitting materials. Even as white light sources they were shown to reach efficiencies comparable or better than fluorescent tubes. The principle beside these devices is very simple: charges (electrons and holes) are injected from the electrical contacts into the organic layers, where they interact and recombine emitting photons. This phenomenon is called electroluminescence (EL), to distinguish it from other kinds of luminescence being produced by different sort of excitations (optical, thermal, chemical, etc.).

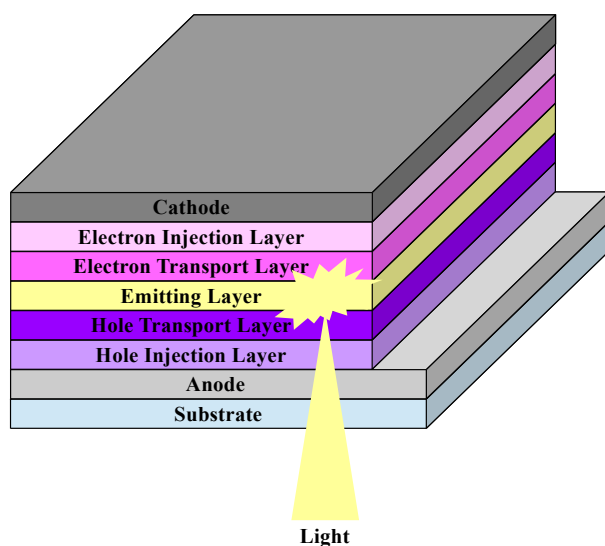


**Figure 1.12** - Schematic of a bottom up OLED structures

In OLEDs structure at least one of the electrodes must be transparent in order to make the light visible from outside. Depending on the position of transparent electrode, we can have two different device configurations. The most common device structure is called bottom-emitting architecture, using the transparent electrode between the device and the transparent substrate (typically glass, but also plastic materials as PEN or PET have been exploited), making the other electrode of highly reflective metals deposited over the organic

layers on the top of the structure. The other architecture, known as top emitting, can be obtained reversing electrodes properties; i.e. the top contact must be transparent. This solution is less used because of the technological issues connected to the realization and patterning of a transparent conductive layer (very thin metal layers or Transparent Conductive Oxide TCO) without damaging the previously deposited organic layers.

OLEDs can also be classified depending on the molecular weight of the employed organic semiconductor. Small molecules OLEDs (SMOLED) have been exploited first [6]. The most used technique to deposit Small molecules OLEDs is thermal evaporation in high vacuum. Typically complex multilayer systems are used to reach high device efficiency, where various functions like charge transport, recombination, etc. are performed by different materials.

A schematic description of small molecules multilayer OLED with the function of each layer has been reported in figure 1.11. Obviously not always all the depicted layers are present, because the different functions may be combined in one material [7].

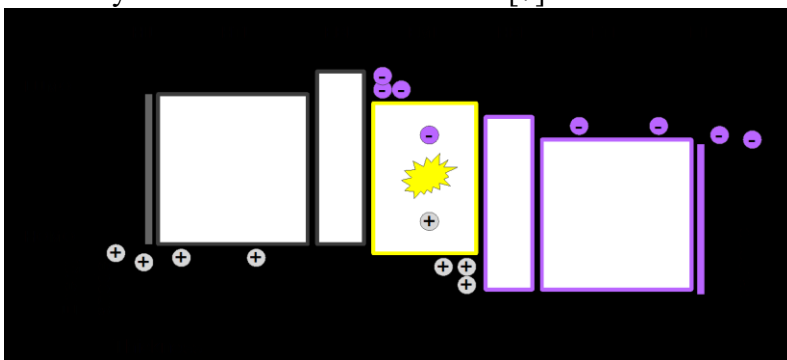


**Figure 1.13** - General multi-layer sequence for small molecules OLEDs.

The Emission Layer (EML) is generally located in the middle of the device and has the function to let carriers interact among each other (recombine) in order to emit light. The recombination process involves the formation of an excited molecular state known as exciton. The more excitons are allowed to decay radiatively, the more the device efficiency will be improved.

Before reaching the EML, holes are injected from a high work function anode into the HOMO level of an organic semiconductor having a comparably high hole mobility (the Hole Transport Layer, HTL). On the other side of the device, electrons are injected from a

low work function cathode into an organic material with high electron mobility (the Electron Transport Layer ETL). Usually ITO (transparent and conductive oxide) is used with good results as anode electrode and it is a common choice in bottom-emission layout. On the cathode side the more suited metals, but prone to degradation, are calcium, magnesium or cesium. Often these materials are used combined with more stable aluminum or silver.

In order to improve the injection, a thin Hole Injection Layer (HIL), can lower the energy barrier between anode and HTL HOMO level. Electron Injection Layer (EIL) performs the same purpose for electrons. To further improve injection and transport, electrical doping of HTL and/or ETL can be applied as well. Before getting to the EML, holes can pass through another layer, the Electron Blocking Layer (EBL). In the same way, electrons have to pass through a Hole Blocking Layer (HBL). EBL and HBL are not always present in the device structure but at the same time they are often important to reach high device efficiencies. Three fundamental functions are performed by blocking layers:

- prevent leakage of the opposite charge carrier type from the EML into the transport layers, forming heterojunction energy barriers in the LUMO-HOMO levels;
- spatially separate the excitons in the EML from doped HTL-ETL (because dopants often act as effective luminescence quenchers, forcing a non-radiatively decay of excitons);
- realize exciton confinement in the EML.

Polymer OLEDs, differently from small molecules devices, are typically processed through spinning or different coating deposition techniques, where the solvent is removed by annealing steps.

Polymer devices are limited in their complexity because of the used solvents that are frequently harmful for the underlying layers. Simple structures employing only a single active layer, where various materials having different functionalities are blended, sandwiched between the electrodes are often used.

In order to improve the general complexity of wet-processed devices, tremendous efforts are spent on improving polymer processing. These efforts include the use of cross-linking polymers to enable deposition of sequential layers from solution, cross-linking in

connection with direct photolithography to achieve patterned polymer layers, and the laser-induced forward transfer of individual device pixels. Besides these uniform coating techniques, printing techniques, derived from publishing, can be used to process polymer-based devices. A compromise is often found in the combination of solution processes and thermal evaporation to achieve multilayer OLEDs that partially consist of layers that comprise solely low molecular weight materials. Finally, similar to small molecules OLEDs, the preparation of the highly reflective cathode requires thermal evaporation in high vacuum [7].

## 1.5 Degradation of OLED Devices

Despite all the advantages shown by Organic Electronics the most critical issue is devices short lifetime that makes them not suitable for large commercialization. This is especially true for OLEDs. Typically, OLEDs degradation can be induced by two different and independent mechanisms: extrinsic or intrinsic degradation [8] [9]. Extrinsic degradation is strictly connected to the rapid degradation of both organic layers and low-work function metals that suffer when they are exposed to atmospheric oxygen and water vapor. Such deterioration leads to the generation of non-emissive regions, also known as dark spots (Figure 1.14), that lead to a decrease in luminance as a result of losses in the emissive area of the device [10] [11].



**Figure 1.14** - Dark spot formation

The main cause of such degradation is connected to the cathode. Either the low work function cathode corrodes and obstructs further

injection or it delaminates from the organic stack. As has been observed, water is more critical than oxygen for OLEDs because water reacts and the releasing hydrogen gas that accumulating beneath the cathode, forces the metal to delaminate leading to the “bubbling” or “domelike” structure often observed in OLED cathode [8] [12].

In order to control extrinsic degradation, a proper protection of the devices is essential. The protection is realized isolating the devices from the environment using barrier materials; such method is known as *encapsulation*. This technique remains still a challenge, especially in the case of devices deposited on flexible substrates. In fact, materials used for the encapsulation system must assure transparency, flexibility and extremely low values of gas transmission rate, particularly water vapor (WVTR, Water Vapor Transmission Rate), such to ensure acceptable lifetime of the devices for commercial use.

As pointed out before, higher sensibility of OLEDs against water vapor than oxygen has been observed, so WVTR is mostly used as a barrier criterion [13]. Proper design of the encapsulation system is strictly required taking into account the relative sensitivity of the specific device to the atmospheric environment (OLED, OPV, OTFT), the type of substrate support (flexible or rigid) and the operating conditions.

The other degradation mode, intrinsic degradation, refers to the progressive decrease of the luminance over time without any other evidence of degradation in the device appearance. The understanding of the origins of the intrinsic degradation still remains a challenge and up to now, only few mechanisms have been proposed to describe intrinsic degradation. Unlike the previous mechanism, which is essentially attributed to external factors, and involve processes that are independent from the specific organic material system, intrinsic degradation is primarily material dependent. Thus, although some of the few mechanisms that have been identified for a particular material system are expected to extend to other systems, experimentation has yet to prove that [8].

Until now the proposed mechanisms to explain intrinsic degradation involve some unrelated factors that include: (i) morphological and thermal instability (any changes in the bulk properties of emissive layer can affect the radiative recombination), (ii) trap formation (interfacial trapped charges affect the electric field distribution and hence the injection properties), (iii) anode instability

(any changes in the injection contact will affect the carrier injection efficiency and hence the carrier profile) [9]. In these mechanisms, the decrease in the electroluminescence has been observed during device operation.

Nowadays this represents the most open issue in the field of OLED degradation research, depending both on the complexity of the phenomena and on the relative novelty of the topic.

In the following sections extrinsic degradation mechanism and relative solution will be presented first. The comprehension of this phenomenon is unavoidable to face the study of mechanism behind more complex intrinsic degradation.

## Chapter 2

# 2 Principle of permeation and barrier technology

In order to understand the degradation mechanism and to study the permeation through polymeric materials (organic) and hybrid systems (organic-inorganic), it is essential to describe the basic physical background of permeation. In this chapter has been described first the basic principle of permeation. Then measurement techniques for ultra-low values of WVTR are presented. Finally the most used solution, for barrier encapsulation technologies, together with some of the most used barrier deposition technique are displayed in the subsequent sections.

### 2.1. Principle of permeation

Permeation is the mass transport of a gas or liquid, the permeate, through a solid. Permeation is a very complex process consisting of three separated phases [14] known as:

- adsorption: from the high concentration area the permeate is adsorbed at the surface in contact with the solid and dissolved into it.
- diffusion: The permeate diffuses through the solid in a random-walk through diffusive jump.
- desorption: The permeate is desorbed from the surface of the solid from the low concentration area.

Assuming constant the concentration gradient, the diffusion process then requires some time to reach a steady state, time needed for the saturation of available space within the polymer for the diffusion.

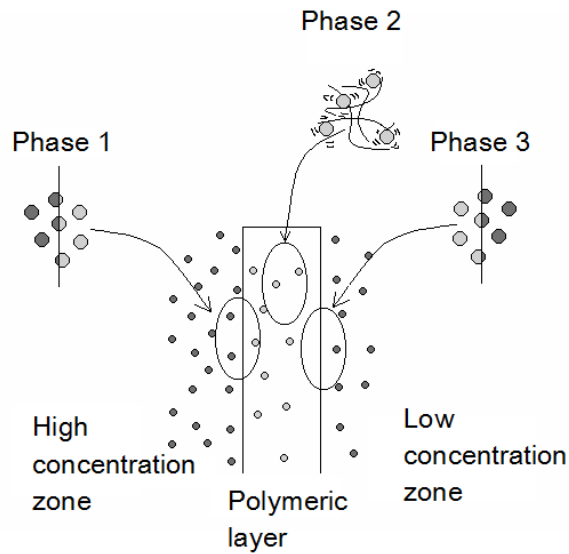


**Figure 2.1** - Schematic of the permeation process

### 2.1.1 Adsorption and desorption

Adsorption phase is the process of gas bonding on the surface. Either weak or strong bond are possible on the surface. On the other side desorption is the release of the gas from the surface. Since the gas molecules are bonded to the surface, an activation energy is needed for desorption. At room temperature only gases bonded by weak bond can be desorbed.

The equilibrium concentration of the sorbed penetrant  $c$ , can be related to the ambient pressure  $p$  by:

$$c = S(c, p)p \quad (2.1)$$

where the solubility coefficient  $S(c, p)$  is a function of  $p$  and could be described by several sorption models [15]. For an ideal system and low concentration of sorbed penetrant,  $S$  can be described by Henry's law and is independent from  $p$  and  $c$ . In this case, the relation between  $c$  and  $p$  (isotherm plot) results linear. For non-ideal systems the absorption isotherm is generally non-linear. Some possible non-linear isotherms are showed in Figure. 2.2.

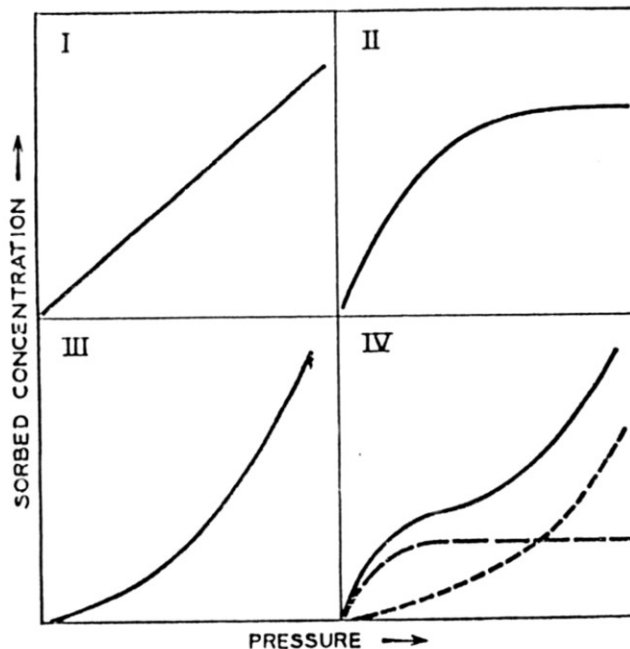


**Figure 2.2** - Typical isotherm plots of sorbed concentration versus ambient vapour pressure: (I) Henry's law; (II) Langmuir equation; (III) Flory-Huggins equation; (IV) BET equation [16].

### 2.1.2 Diffusion

Diffusion is the directed mass transport of randomly moving particles [17]. It is induced by a gradient of concentration. Diffusion can occur via defects, like micro-cracks, or through the bulk material itself. Diffusion through the bulk is negligible for inorganic materials, because their bulk diffusion coefficients are orders of magnitude

lower than their effective diffusion coefficients as a result of defects in the material structure. On the contrary, diffusion through the bulk material is an important issue for polymers. The particles can be seen as jumping from one site to another passing over a potential barrier separating one position from the next. These positions can result from a rearrangement of the polymer chains. This is possible for polymers at room temperature because the polymer chains stick together via weak van-der-Waals-bonds and the activation energy needed for a rearrangement is therefore low. The diffusion through polymers is much more important than the sorption, and consequently limits the permeation [18]. Thus, permeate concentrations at the surfaces are defined only by the sorption and can be treated as constant for diffusion calculations.

Diffusion through a homogeneous diffusion medium, meaning polymers but not inorganic barrier layers, is described by Fick's laws. Fick's first law of diffusion describes the flux in z-direction depending on a concentration gradient at any point or plane in the diffusion medium [17]:

$$J = -D_z \left( \frac{\partial c}{\partial z} \right) \quad (2.2)$$

where J is flux of the permeate, D (cm<sup>2</sup> s<sup>-1</sup>) is the diffusion coefficient also indicated as Fick's coefficient.

### 2.1.3 Permeation

Combining Fick's first law with the continuity equation Fick's second law of diffusion is obtained. It describes the evolution of the permeant concentration over time [17]:

$$\frac{\partial c}{\partial t} = -D_z \left( \frac{\partial^2 c}{\partial z^2} \right) \quad (2.3)$$

These equations are fundamental for unidirectional diffusion in an isotropic continuum when the diffusion coefficient D is constant and independent from z, t or c. Actually in many penetrant-polymer systems D is not a constant but is a function of c, the spatial

coordinates and  $t$ . Anyway most commonly  $D$  is only dependent on the sorbed penetrant concentration.

When Henry's law is obeyed, using it in the equation for the flux it has been derived:

$$J = DS \frac{\Delta p}{z} \quad (2.4)$$

where  $\Delta p$  is the difference between partial pressure over the substrate and  $z$  is thickness of the film. The product  $DS$  defines the permeability coefficient  $P$ , so that the relation above becomes:

$$J = P \frac{\Delta p}{z} \quad (2.5)$$

Since the diffusive flux  $J$  can be also defined as the total amount passing through a plane surface of unit area normal to the flow direction during unit time and written as:

$$J = \frac{Q}{At} \quad (2.6)$$

where  $Q$  is the total amount of penetrant which has passed through area  $A$  during time  $t$ . The permeability  $P$  can be then written as:

$$P = \frac{z}{A\Delta p} \frac{\Delta Q}{\Delta t} \quad (2.7)$$

such that the permeability constant can be calculated from linear part of the  $Q$  versus  $t$  curve.

Furthermore when a penetrant diffuses through a polymer film in which it is soluble, there is a transient state from the time the penetrant first enters the film until the steady state is established.  $T$  intercept on the time axis of the extrapolated linear steady state portion of the curve is called lag time,  $L$ .

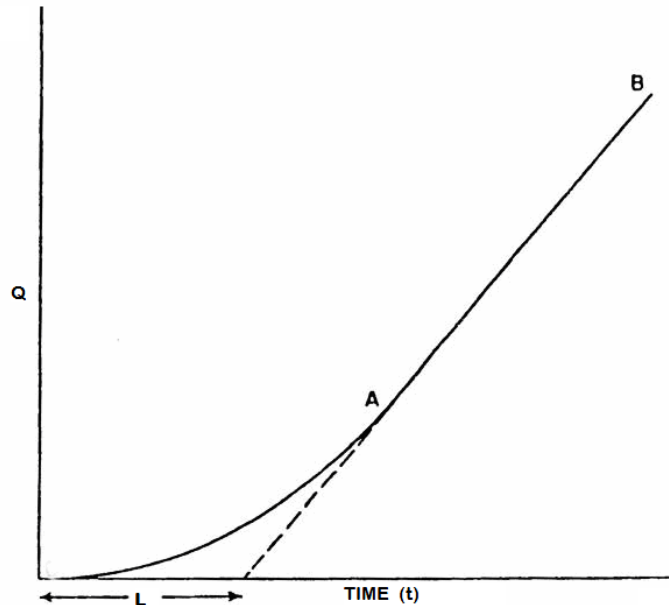


**Figure 2.3** - Typical permeation curve: amount of permeated penetrant  $Q$ , as a function of time,  $t$ .

For the common experimental case when the film is initially free of penetrant and the receiving volume is maintained at essentially zero concentration it has been shown that [19] [20]:

$$L = \frac{z^2}{6D} \quad (2.8)$$

so that all the parameters can be calculated from single experimental curve  $Q$  versus time and in particular  $P$  from the steady state flux,  $D$  from the lag time and  $S$  from the ratio between  $P$  and  $D$ .

The permeability  $P$  also shows a temperature Arrhenius like dependence so that  $P$  can be written as:

$$P(T) = P(0)e^{-\frac{E_A}{k_B T}} \quad (2.9)$$

Where  $P(0)$  is a constant and  $E_A$  is the activation energy. This relation is not valid in all situation, but is valid when the potential seen by the permeate remains constant, meaning that the microscopic structure of

the solid has to remain constant. This is also applicable to polymers in a small range of temperature. This behavior might be ascribed to the diffusion coefficient  $D$  and not to the sorption coefficient  $S$ .

Even if it is possible to measure  $P$  through experimental methods and apparatus, very often it is used the flux through a unit area surface into a unit time of the permeant gas. So if the permeant is water the barrier material is characterized in terms of Water Vapor Transmission Rate (WVTR) measured in  $\text{g m}^{-2} \text{day}^{-1}$ .

## 2.2 Permeation Measurement Techniques

The ultra-high barrier performance requested by organic devices [21] lead to another critical need: ultra-sensitive permeation measurement instruments. Since before the barrier target requested by organic electronic devices, extreme permeation barrier layer has been a niche product, permeation measurement instruments at these ultralow rates are not industry standard yet. Not even the market leader, offers, at his best commercial standard, sensitivity comparable with organic electronic requirements. As a consequence, new permeation measurement methods came up. These methods can be based both on direct measurement principles intrinsically sensitive enough, as well as different measurement methods using electrical or optical signals, weighing, and mass spectrometry or pressure measurements. All measurements require close control of the permeation conditions like temperature or relative humidity. Hence it is useful to define standardized pair of temperature and humidity conditions. Some of the most used are 23 °C 50% RH (ambient), 38 °C 90% RH (tropical), 60 °C 90% RH (accelerated aging), and 85 °C 85% RH (damp-heat test) [13].

Depending on the type of setup used, some are limited in temperature or fixed to certain humidity levels, some methods can be applied only to measure certain gas and some can be used to measure only film-like barrier. On the contrary as is very usual in barrier encapsulation systems, the quality of a perimeter seal needs to be determined and further experimental effort are needed. Care must be taken to interpret and compare either the results, since the measured

rates directly depend on temperature and humidity levels, and the size or the position of the measured area, In the following sections, some methods to measure the WVTR of barriers are presented. Their benefits and drawbacks, as well as their application (only barriers on polymer substrates or even thin film encapsulation system) and range of sensitivity, are discussed.

### 2.2.1 Coulometric Devices

In a coulometric device, the measurement device is divided by the barrier test into two chambers. In one chamber a gas atmosphere of the test gas is maintained with constant temperature and partial pressure. The other chamber is purged with an inert carrier gas such as nitrogen ( $N_2$ ).

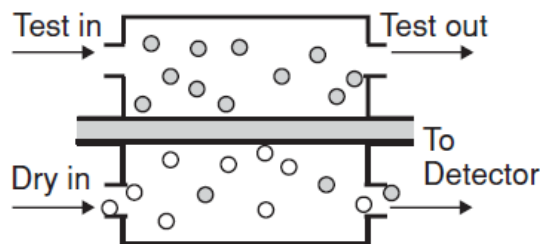


**Figure 2.4** - Principle of water vapor permeation measurement using a carrier gas method such as a coulometric device [13].

The carrier gas is used to transport permeated test gas (usually water) to the sensor. This sensor consists of two adjacent electrodes separated by phosphorus pentoxide ( $P_2O_5$ ).

The principle is based on the dissociation of water molecules when they come in contact with the strongly hygroscopic  $P_2O_5$  material, used as an electrolyte. Applying an electrical field to the two electrodes a current is induced that directly depends on the number of absorbed and dissociated water molecules. This principle can be used also to oxygen measurement and in this case the oxygen detector consists of a graphite cathode and a cadmium anode.

Measurement devices based on this principle have a short measurement time, a wide measurement range and can measure

sample of large area (up to 100 cm<sup>2</sup>). The lower measurement limit of existing prominent coulometric devices is 5 10<sup>-5</sup> g m<sup>-2</sup> day<sup>-1</sup> and is manufactured by Mocon (Aquatran II).

### 2.2.2 Mass Spectrometry

Mass spectroscopy, can be used to detect small traces of various gases, e.g. H<sub>2</sub>O, O<sub>2</sub>, N<sub>2</sub>, and He [22].

There are two general setups to measure gas permeation with a mass spectrometer. In the common setup, the film under test separates two gas cells. One cell contain a high partial pressure of the permeate gas. The other gas cell is kept under ultra-high vacuum (UHV) and is connected to a mass spectrometer. In the other configuration a gas cell being covered on one side by the sample, only, is put into a vacuum chamber that is connected to a mass spectrometer [23].

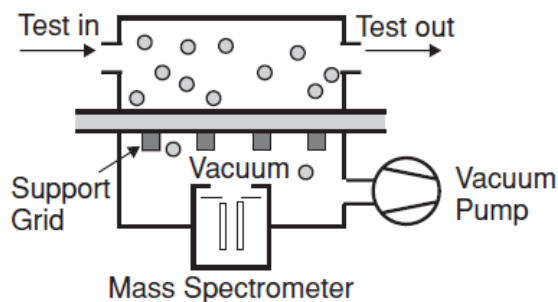


**Figure 2.5** - Setup for mass spectrometric permeation measurement [13].

In the first setup, a constant partial pressure of the test gas will be measured by the mass spectrometer after reaching the steady-state permeation condition.

In the second setup the pressure in the chamber is decreasing over time as the amount of available gas in the gas cell decreases over time as well. For simple gases an exponential decay of the partial pressure over time is observed. The gas transmission rate of the sample can thereby be derived from the exponential decay constant. The most important advantage of mass spectrometric gas permeation measurements is the possibility to test all gases that are detectable with a mass spectrometer. It can be also measured the permeation of different gases and gas mixtures through a sample at the same time

using the same detector, to exploit the interactions between different test gases in a barrier sample. The main drawback of this measurement technique is the complex equipment required for sensitive measurements. The detection limit of the mass spectrometric method for water vapor permeation lies in the range of  $10^{-5} \text{ g m}^{-2} \text{ day}^{-1}$ .

### **2.2.3 Laser absorption**

Using the principle that traces of water or other gases absorb light, a laser beam can be employed to measure the water density either directly behind a barrier foil or in an inert carrier gas stream coming from this foil [24]. Hence, a laser beam with a wavelength which would excite water loses intensity when propagating through a volume containing water vapor. Consequently, based on water density, the WVTR of this barrier foil can be calculated. In practical application terms, the detection limit is defined by the quality of the barrier foil sealing. The detection limit for water vapor permeation ranges from  $10^{-4} \text{ g m}^{-2} \text{ day}^{-1}$  and  $10^{-6} \text{ g m}^{-2} \text{ day}^{-1}$  [24].

### **2.2.4 Calcium Corrosion Tests**

Calcium Test is probably the most widely employed and the easiest technique for the study and evaluation of barrier properties exhibited by the materials used for encapsulation, although it is an indirect method and not yet standardized. The basic principle relies on the observation of chemical transformation of a thin film of metallic Calcium changing its characteristics from conductive and opaque to an hydroxide nonconductive and transparent. The permeation can be tested evaporating on a substrate the Calcium thin film and immediately protecting it (encapsulation process) in an inert environment by the barrier material of which we want to know the permeability and measuring the change in the electrical or optical properties. If exposed to environmental oxygen and water vapor, calcium can react, at least at low temperatures ( $<150^\circ \text{ C}$ ), with only the water permeating through the barrier material according to the following reaction [25] [26] [27]:



Leaving the prepared device exposed to known and constant environmental conditions, metallic calcium becomes calcium hydroxide with the progress of time (and consequently the permeation of water vapor within the encapsulation system), passing from to be a reflective (and conductive) to a transparent (and insulating) material.

Therefore, monitoring the variation of these properties over time, it is possible to calculate, by means of suitable mathematical models, the amount of water permeated through the barrier material. So, by measuring changing in the electrical resistivity or in the optical absorption coefficient of the calcium layer, it is possible to discern between *electrical* or *optical* calcium corrosion tests respectively.

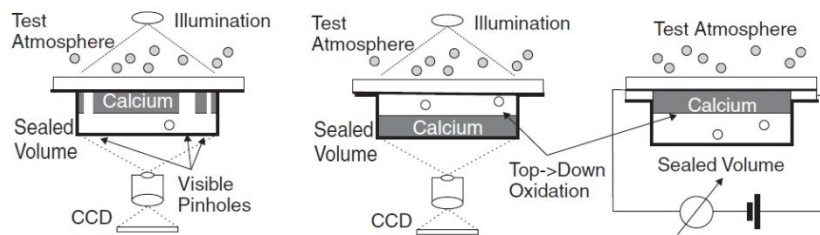


**Figure 2.6** - Different calcium test setups. The conversion of calcium (Ca) can be monitored by optical transmission (left and center) or by electrical resistance measurements (right). For both principles, two variants are possible: placing the Ca layer directly on the barrier (left) causes local Ca conversion at barrier pinholes and thereby allows the characterization of pinhole sizes and densities. Placing the calcium layer with a connecting gas volume causes evenly distributed Ca consumption (center and right) [13].

This method is ideal for the long-lasting experiments, able to evaluate the effective WVTR (including the macro-defects caused by the processing of the barrier, fundamental to check the quality and hence improve the process itself) with very good accuracy and at relatively low cost setup. Another advantage of measurement devices based on this principle is the high versatility: theoretically Calcium Test can be used with a huge variety of geometries. It also offers the possibility to test in a configuration similar to the device configuration. The major drawback is the difficulty to compare results from different research groups or laboratories.

The limit of the Ca test sensitivity depends on the setup, but is assumed to be in the  $10^{-6}$  g m<sup>-2</sup> day<sup>-1</sup>) range [28] [29].

## 2.3 Barrier Requirements

As told in the previous chapter, organics devices suffer the exposure to environmental oxygen and water vapor. Thus the protection of organic materials from surrounding environment remains a strong necessity and a tough technological challenge. This protection is known as encapsulation. Encapsulation requirements depend on used materials sensitivity, specific product (OLED, OPV, OTFT), type of substrate and environmental operation condition. Particularly, OLED represents the worst case in terms of sensitivity to environmental conditions.

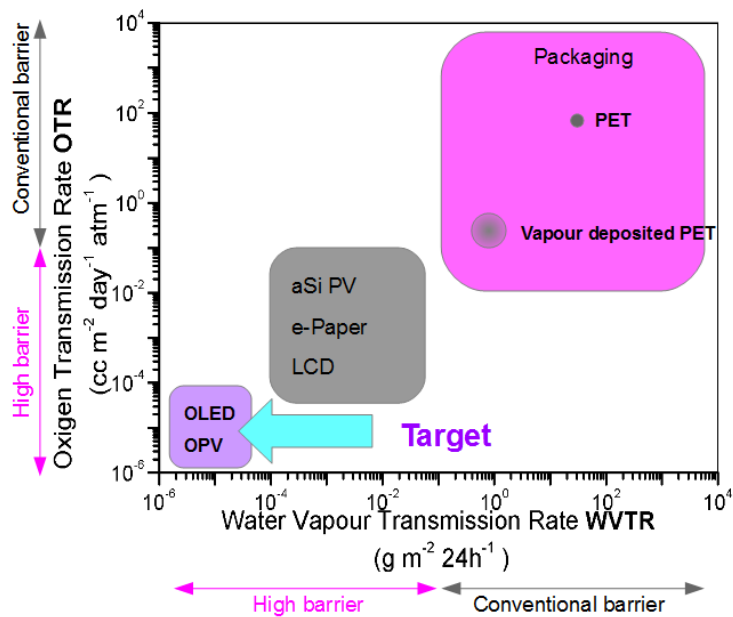


**Figure 2.7** - Requirements in terms of WVTR (x axis) and (y axis) for various commercial areas

The requirement for a barrier with a water vapor transmission rate of  $10^{-6} \text{ g m}^{-2} \text{ day}^{-1}$  [10] can be found in many papers about encapsulation of organic electronic devices. This requirement is usually derived for OLEDs, which often include highly reactive low work function metals as cathode. Assuming low work function cathode corrosion as the main responsible for OLEDs degradation, As was made in literature [21] [10], it is possible to calculate the amount of g ( $\text{H}_2\text{O}$ ) needed to degrade the devices. From these calculations OLED devices requires barriers in the range of  $10^{-6} \text{ g m}^{-2} \text{ day}^{-1}$  in terms of WVTR, to assure a reasonable life of the devices. In the same context, a 1000 times higher sensibility of OLEDs against water vapor than oxygen has been observed, so the water vapor transmission rate (WVTR) is widely used as a barrier criterion [13]. This criterion has been also stated to assure 10000 hours of operation [30] [8] even if devices encapsulated with barrier materials with WVTR values of  $10^{-6} \text{ g m}^{-2} \text{ day}^{-1}$  have anyway shown shorter lifetime [21]. Actually an exact relation between operation hours and WVTR barrier value has not been demonstrated especially due to the complexity of OLED architectures and variety of the materials employed.

## 2.4 Encapsulation solutions

As discussed before, to protect an organic device from ambient gases is essential. Barriers have to be applied on all sides of the device and they must have some precise characteristics, apart from the barrier value, such as transparency or easy and cheap manufacture process. Typically encapsulation can be classified depending on the type of substrate, the relative sensitivity of the device (OLED, OTFT, OPV) and the operation condition of the specific application. In the subsequent sections are described the basic principles of the possible solutions.

### 2.4.1 Glass to glass approach

When the device is realized on glass substrate the best solution is represented by the use of a hard lid of glass. The glass cover is then sealed with substrate by means of an UV-curable epoxy resin, in an inert atmosphere. It is also possible to add a dehydrating agent (getter) between cover and device inside the sealed volume. Macroscopically thick glass sheets are practically a perfect barrier against oxygen and moisture, they also withstand chemicals and temperatures, are highly transparent and easy to handle in small pieces.

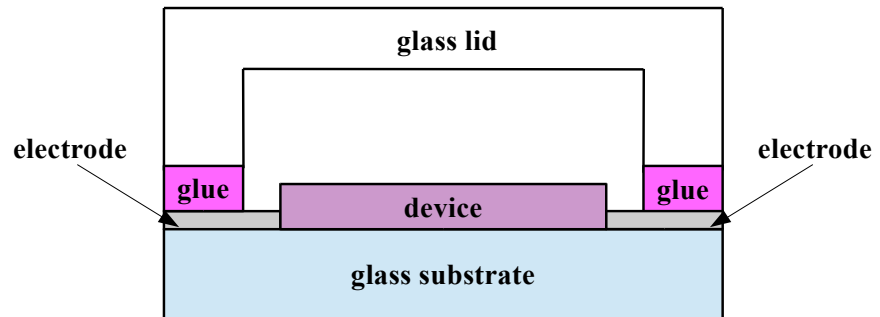


**Figure 2.8** - Schematic of a glass to glass encapsulation system with getter added within the volume

However, since glass is brittle, heavy, and rigid, it is unfavorable for example for large-area devices and portable applications.

In this encapsulation approach, the permeating surface is represented by the sealing epoxy resin surface that also represents the weak point of this technique. Hence in this case the major challenge consists in the identification of a high impermeable resin, the minimization of the permeating surface and the optimization of the UV curing process. In literature, for glass-glass encapsulation system has been reported WVTR values in the range of  $10^{-6} \text{ g m}^{-2} \text{ day}^{-1}$ . Up to now glass to glass encapsulation is still the most stable and most reliable encapsulation technology available and is widely used as reference for permeation and device measurements.

### 2.4.2 Lamination of film barrier

A valid alternative to the rigid glass to glass encapsulation is the lamination of barrier films. The device can be realized directly on the barrier film and then laminated with another barrier film. The whole processing of a device can be done in a roll-to-roll configuration, Thus since roll-to-roll processing requires the barrier films to be flexible, this limits the thickness of barrier films in order to avoid mechanical stress and delamination. The barrier coatings are joined using special adhesives, usually applied on the complete device area and have similar permeation issues as the glass to glass sealing surface even if the adhesive sealing is exposed to more mechanical stress than on glass due to the flexible substrate and needs to be optimized.

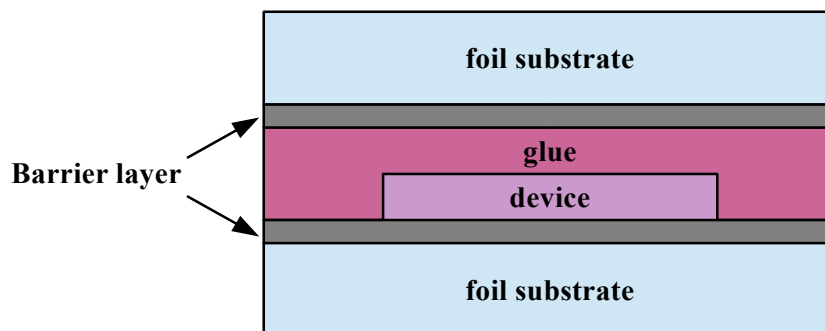


**Figure 2.9** - Schematic of an encapsulation system with barrier layer laminated on the device surface

Using the lamination technique the barrier layer can be processed separately from the organic device so that aggressive processes, such as high temperatures, radiation, chemical baths and gases, can be applied for the production of the barrier film. Anyway if the device is processed on top of the barrier film, the barrier must not be damaged during the subsequent processes, which are especially critical for patterning steps by laser ablation or wet etching. In general, flexible barrier coatings are thin and sensitive to mechanical strain and surface damage, so large-area manufacturing, handling and lamination present a technological challenge.

### 2.4.3 Thin Film Encapsulation

In order to reduce mechanical stress and abrasion to the barrier, to limit the issues connected with the distance between barrier film and sensitive area and to minimize the process steps and cost the Thin Film Encapsulation (TFE) technique has been developed. Using TFE after the device realization on a substrate, it is sealed applying the film barrier directly on device surface.

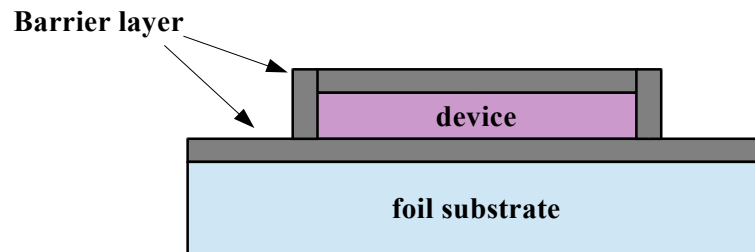


**Figure 2.10** - Schematic of an encapsulation system realized with the Thin Film approach

Thus parasitic effects and device contamination can be reduced and damage due to a separate mechanical lamination process is avoided. The main issue of TFE is the need to process on the organic device, which severely limits the processing conditions. Therefore many technologies, using plasma, reactive gases or high temperatures to achieve dense inorganic barrier layers are difficult to use in thin-film encapsulation processes.

Typical TFE processes involve deposition of an inorganic barrier film, mostly oxides or nitrides from different vacuum deposition techniques. Some of the most used are:

#### Sputtering

Sputtering is the most often used technology for the deposition of barrier layers for the encapsulation of flexible electronic devices. Permeation barrier properties superior to evaporated layers can be achieved with using a sputtering process [31] [32]. In this technique a sputtering target is bonded onto a cooling plate. The cooling plate is

water cooled on the backside to avoid thermal damage to the target. The sputtering target itself acts as cathode and a negative voltage is applied to it, accelerating sputter gas ions to the target surface after the plasma has been ignited. Often, rectangular magnetrons are used to deposit sputtered oxide or nitride barrier layers. For metallic target typically a direct current (DC) or a pulsed DC power supply is used. Pulsing the plasma voltage leads to improved process stability. If the target material is nonconductive (such as most oxide targets) DC sputtering cannot be used. In this case a radio-frequency (RF) power supply is required. RF processes typically have a lower deposition rate compared to DC or pulsed DC sputtering. However, with all sputtering modes barrier layers with low water vapor and oxygen permeation can be deposited.

#### Plasma-Enhanced Chemical Vapor Deposition (PECVD)

Another common method to deposit barrier layers on polymer webs and also directly on devices is a PECVD process. Plasma is used to provide the activation energy for a chemical reaction between different reactants (precursor gases) that finally will precipitate on the substrate as a thin layer. Lower substrate temperatures are possible with plasma CVD in comparison to other CVD processes.

This feature makes PECVD the favorable CVD process, since the thermal stability of typical substrates such as PET (or organic electronic devices themselves) is very limited often to less than 150 °C. Among the typically used plasma sources for PECVD a very often used and simple setup is the capacitive radio frequency PECVD reactor. Radio-frequency PECVD is mostly used to deposit SiO<sub>2</sub> or SiN<sub>x</sub> barrier layers in a batch coating process. Another method for generating dense PECVD plasma is a magnetron or dual-magnetron system. However, large-area Magnetron-PECVD coatings and the application of this process for the deposition permeation barrier layers were propagated first a few years ago [33] [34]. As magnetrons are available for a large coating width already, this process can easily be scaled to larger coating areas [35].

#### Atomic-Layer Deposition (ALD)

The atomic-layer deposition (ALD) process is a special process that can be used to produce very dense almost defect-free thin films on different substrates [36]. Sometimes, ALD is also referred to as

atomic-layer epitaxy (ALE) [37]. The ALD process is based on the cyclic alternating injection of two different reactants into a processing-coating chamber with intermediate purging steps. Different steps of a typical ALD cycle are illustrated in Figure 2.11. One cycle begins with injecting a first highly reactive precursor-reactant. The reactant will precipitate onto the substrate and the coating chamber walls. In a second step, the coating chamber is purged with an inert gas for a certain (longer) time to remove residual precursor material leaving only a monolayer on the substrate and the chamber walls. The third step is the injection of a second reactant that reacts on the substrate surface with the first reactant forming usually less than a monolayer of solid oxide material. Finally, another purging step is needed to clean the process chamber from the second reactant before starting the next cycle.

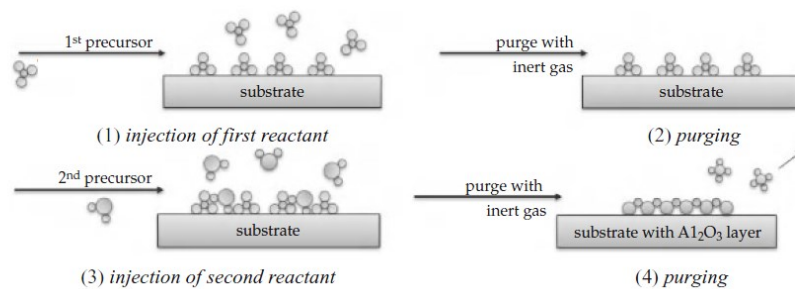


**Figure 2.11** - Various steps of one ALD cycle for the deposition of an  $\text{Al}_2\text{O}_3$  monolayer [13]

The most time-consuming steps within an ALD cycle are the purging steps as it needs to make sure that all residual precursor gas is removed from the substrate and the process chamber before the second precursor is injected. Typical cycle times are in the range of one to a few minutes, whereas the reactants are injected for less than one second and purging is done for about 30 to 60 s at an elevated substrate temperature between 100 °C and 175 °C for  $\text{Al}_2\text{O}_3$  coatings [36] [38]. At a lower substrate temperature higher purging times are required to achieve a good layer quality. One of the most important properties of the ALD technology is the self-limitation of the reaction which means that the deposition rate is equal to or less than a monolayer for each cycle, leading to an ideal layer-by-layer growth.

Because of this ALD layers have a very high density and a very low number of defects [37]. However, the major drawback of the ALD process is its very low deposition rate and productivity.

Just like barrier films, multiple layers can be stacked to improve barrier properties.

### 2.4.3.1 Permeation through single thin film

Different materials are used for thin film encapsulation of organic electronic devices each of them showing its own permeation mechanism. Permeation process through polymer films used as substrate can be well described using Fick's laws of diffusion. Unfortunately, as is widely known, polymers do not have a sufficiently low water vapor and oxygen permeation to be used as sole encapsulation for organic device. Typical values of WVTR, for polymer films at 38°C and 90 RH, range from 1 to  $10^{-2}$  g m<sup>-2</sup> day<sup>-1</sup>. These values are far from requirements for organic electronics devices.

On the other hand inorganic materials are in principle completely impermeable, even if they have a lot of drawbacks such as mechanical ruggedness, and the costly vacuum deposition processes. Actually theoretical permeation is several order magnitude lower than the measured one. This is due to the presence of defects in the material structure. These defects are considered as almost solely responsible for the permeation of gases through the thin films, while the Fickian solid state diffusion is negligible [14] [39].

These irregularities mainly result from substrate surface roughness also due to particles like dust leftovers on the substrate [38], or particles generated during the deposition process [40]. Using the Arrhenius dependence of permeation from T is possible to investigate how the defects dominate the barrier performances. Particularly it is possible to relate the activation energy of permeation with the nature of defects [41]. According to the geometry, it is possible to classify the defect in *macro-defects* (diameter above 1nm), *nano-defect* (diameter between 0,3 and 1nm) and *lattice interstices* (diameter below 0,3 nm) [42] as showed in Figure 2.12.

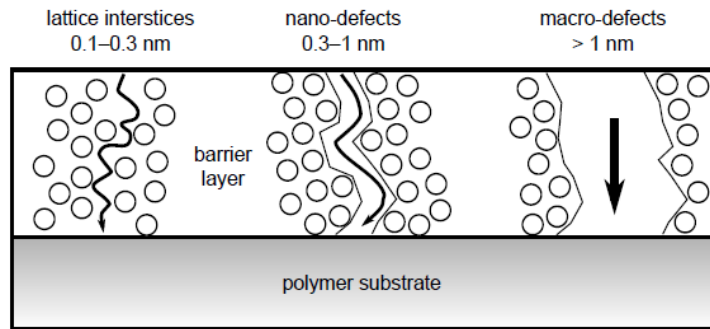


**Figure 2.12** - Classification of defects [42]: permeation of water and oxygen through barrier layers is dominated by nano- and macro-defects. Lattice interstices are too small for both of them.

Comparing the permeation through bare substrate with the one through substrate-covered with the barrier layer it is possible either to find the same activation energy for both or an elevated one. In the first case the barrier layer acts simply as a block reducing the effective area for permeation while in case of an interaction with the inorganic layer, elevated activation energy is expected. If the activation energy is the same for the barrier material as for permeation through the bare substrate, permeate flow through macro defects there is no interaction with the barrier material. On the other hand, very high activation energy reveals the presence of defects with a diameter below 0.3 nm (lattice interstices). Of special interest are the nano defects between 0.3 and 1 nm. Permeate-flux through those defects is characterized by an interaction with the barrier material and, consequently, increased activation energy when compared to the substrate.

Hence, the activation energy reveals the nature of permeation: Activation energy as low as for the bare polymer substrate proves that permeation is dominated by macro-defects without interaction with the barrier layer. An activation energy as high as the bulk barrier material proves the absence of macro defects. Any activation energy between the one for the polymer and the one for the bulk barrier material refers to a mixture of both cases. [42].

The behavior of polymer and oxide lead to the adoption of barrier coated polymer films. The permeation through coated polymer webs and multilayer stacks as well as the interactions between the different layers and the substrate is described through several models.

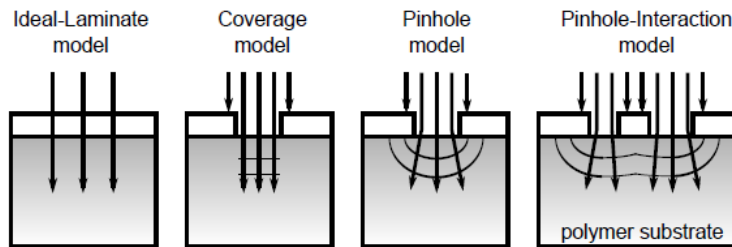


**Figure 2.13** - Most used models employed to explain permeation through single thin films on polymer substrates [13]. In all models, except for the Ideal-Laminate model, permeation occurs solely through pinholes with the barrier acting as an inert block.

The simplest one is the *ideal-laminate* theory as illustrated in Figure 2.13 [39] [14]. This model is based on the assumptions that all layers are permeable with a permeation coefficient other than zero ( $P_1 P_2 \dots P_n \neq 0$ ) and all layers are free of accelerated diffusion paths such as defects.

In that case, the permeation through a multilayer can be described in a similar way as the electrical current in a series of electrical resistances so that the total permeation of the stack can be described through the following equation:

$$\frac{L_{stack}}{P_{stack}} = \sum_{i=1}^n \frac{L_i}{P_i} \quad (2.11)$$

Another simple model is the *coverage model* that is used to describe the permeation through a single layer on a polymer substrate with the assumptions that the permeation through the barrier layer only takes place at defects while the layer material itself is impermeable and that the substrate material is permeable and the permeate is passing unidirectionally through the substrate without distributing itself within the polymer.

With these simplifications the gas flux through the system can be determined using the ratio between the uncovered substrate surface area and the total surface area that is covered with the barrier layer.

To take into account the fact that, in reality once permeated, the permeate will spread in all directions within the substrate material after passing a defect in the barrier layer, the coverage model has been

extended [43] to the *pinhole model*. This model takes into account the three-dimensional diffusion of the permeate within the substrate. While the pinhole model holds true for defect distances 3 times as large as the substrate thickness [44], smaller defect distances reduce the overall permeation and are taken into account in the *pinhole-interaction model*.

#### 2.4.4 Multilayer approach

Since single thin films permeation barriers reached WVTRs are far from requirements for organic electronics devices, solutions for reducing at minimum the presence of defects in the single layer have been exploited. One of the most promising methods includes the realization of multilayer alternating one inorganic barrier layer and one polymer top coat on the barrier [14]. Every pair of polymer and barrier film is typically named *dyad* and most multilayer barriers are built of several dyads. In a multilayer barrier the inorganic layer provides the barrier performance while the polymer layer fulfills multiple tasks. First the polymeric layer has a *smoothing* effect covering the defects in a barrier layer. Hence, a defect or a surface irregularity in one barrier layer does not cause a defect in the subsequent one. This lead also to another positive effect: the path for the permeate to enter the device is extended and the diffusion is reduced (Figure 2.14.), because defects of successive layers are spatially separated. The *tortuous path* cannot lower the steady-state WVTR significantly; but it can shift the lag time to several years [14].

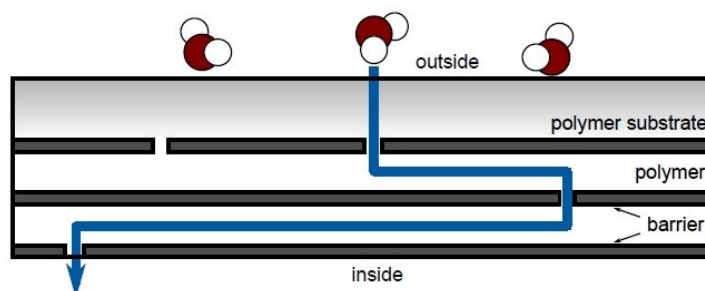


**Figure 2.14** - Tortuous path model: thanks to smooth polymer interlayers, defects of successive layers are spatially separated. The longer distance lowers the speed of diffusion and increases the lag time [14].

Furthermore covering the barrier layers with polymers protects them to some degree against abrasion, scratches, and corrosion. This barrier layer *protection* effect improves the long-term stability. Then using a polymer to fill the defects reduces the diffusion since the defect has no direct air contact. Another advantage regards the *improvement of mechanical flexibility*. Thin oxide layers are more flexible (in terms of bending and strain) than thick layers. Using two thin layers with a flexible polymer interlayer allows a smaller bending radius as well as larger strain or expansion without cracking [45].

The gas permeation through multilayer barriers using the ‘tortuous path of diffusion’ model has been widely discussed in literature assuming that [14] [44]:

- the multilayer barrier consists of at least two inorganic barrier layers with a given average defect distance ( $s$ ) that are separated by a polymer interlayer (which can also be a polymer substrate coated on both sides);
- the permeation through the barrier layers only takes place at defects with the defect distance  $s$ ;
- the interlayer is permeable but free of accelerated diffusion paths (defects). The gas diffusion coefficient of the polymer material is constant over the complete polymer layer thickness ( $d_p$ );
- the distance between two defects within a barrier layer is much higher than the interlayer thickness ( $s \gg d_p$ ).

When all these requirements are fulfilled, the effective path of diffusion through the multilayer barrier is hindered by the large distance between the defects in the barrier layers (Figure 2.15.).

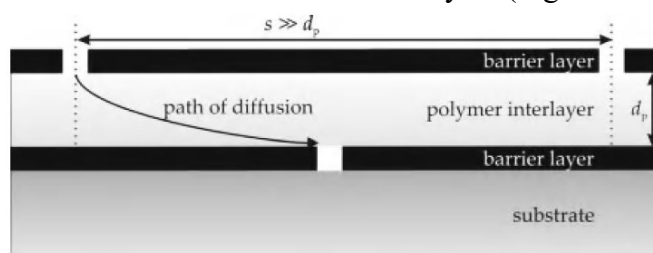


**Figure 2.15** - Schematic illustration of the effective diffusional thickness  $l$  of the polymer layer. This results in a path length which is much longer than the polymer physical thickness  $d_p$  [14]

The gas permeation through multilayer barriers with  $n$  dyads of inorganic-polymer taking into account the time dependence of gas permeation through the layers lead to multiple effects [14]:

- the lag time increases with the number of dyads in the layer stack.
- increasing the defect distance (lowering the defect density) by a factor of 10 leads to an increase of the lag time also by a factor of ten.
- the steady-state permeation through a three- or more layer stack is almost the same as calculated using the ideal-laminate theory.
- polymers with intrinsic barrier properties (lower gas diffusion coefficient) reduce the steady-state permeation through the layer stack [44].
- the gas permeation may be reduced by using thinner polymer interlayers as long as the interlayer is thick enough to maintain its smoothing and defect-covering properties.
- the lag time may be increased up to several years with using 4 or more dyads and with a low defect density in the barrier layers. This lag time may be sufficiently long to allow the encapsulation of long-living organic electronic devices.

The main drawback of multilayer barriers is their price, due to the high amount of effort needed to deposit several barrier layers. Another important issue is delamination. This is due to thermally induced mechanical stresses and low adhesion strength between inorganic and organic layers [46]. However, for adapting to the specifications of organic devices, multilayer-barriers appear to be the best choice.

## Chapter 3

# 3 Development of an Electrical Calcium Corrosion Test measurement system

As shown in the previous chapter, organic devices need very high barrier performance against environmental agents. However, even if very recently a few ultra-sensitive permeation measurement instruments (able to measure WVTR  $< 10^{-3} \text{ g m}^{-2} \text{ day}^{-1}$ ) are available on the market they are really expensive and complex. These measurement systems also show another important drawback; they are able to analyze only film-like barrier, while it is not possible to measure device-like structure. As a consequence, with the fast spreading of the organic devices, custom lab solutions have grown over last decade, such as the calcium test [47]. Calcium corrosion test probably represent the most simple and common technique to investigate ultra-high permeation barriers. In this chapter the corrosion Calcium test developed during this work thesis has been described.

### 3.1 Electrical Calcium test choice

The first part of this work has been dedicated to the practical realization of an electrical calcium tests system. The electrical calcium test has been chosen towards the optical one thanks to some useful features: firstly his elevated accuracy. In fact, even though both methods are based on an indirect measure, the electrical calcium test is based on a resistance measure while optical one is based on a measure

acquired from an image processing that is much more equivocal. Then electrical test requires a simple and inexpensive measurement setup as explained in the following paragraph. This characteristic also gives the chance to perform measures at different temperatures simply placing the sample under different condition.

These temperature measurements result precious both to reduce analysis time but even more important to recognize quantity and dimensions of barrier defects through activation energy evaluation. The same operation would get more difficult using optical calcium test that employs a costly CCD camera.

## **3.2 Layout design**

Even if the principle of the electrical calcium corrosion test is based on a simple resistance measurement, details of the sample layout can strongly influence the measurement. The electrical Ca test device layout designed by ENEA taken carefully into account the most influencing parameters.

### Contact resistance

The resistance of the calcium layer can be precisely measured using 4-wires sensing geometry. In 4-wires sensing geometry one pair of contacts provides the current while the voltage is measured using an independent and thus current-free pair of contacts. Thereby contact resistances are excluded from the measurement.

### Series resistance

The resistance is actually measured between the two voltage-contacts. Since calcium is encapsulated, contacts can not reach the calcium layer directly; they require an electrode on the sample. Generally the electrical resistivity of calcium is comparable to the electrical resistivity of the contact material, and it became important to take into account the series resistance of the electrodes. Hence, a layout with

separate voltage- and current-electrodes has been designed to avoid any influences of series resistance.

#### Contact material

Since the Calcium test measurement has been performed in a climatic chamber, it is possible for the sample and the metal contact, to be exposed to high humidity. In order to avoid possible corrosion problems a noble metal like Silver has been chosen. Even if Silver is more prone to scratches during the probe positioning process on the sample and it shows a brownish effect when the Silver area overlaps the Calcium one, these drawbacks do not affect the measurement and may therefore be acceptable.

#### Evaporation sequence

The evaporation on the barrier material might either start with the calcium or with the electrode deposition. The resistance measurement is not affected by this sequence, while it is supposed to influence the corrosion pattern. Evaporating the calcium first, it is in contact with the permeable material everywhere and corrodes more or less homogeneously. On the contrary if the electrode is evaporated first, it acts like a barrier protecting the calcium evaporated on its top, but also influencing the water path. Consequently, calcium at the edges of the electrode corrodes faster. As the current path is constricted, particularly at this calcium/electrode-border, the current drops fast, leading to a strongly overestimated WVTR and a loss of the sensor while most of the calcium still remains metallic. Hence, the calcium should always be deposited between the electrode and the barrier.

#### Homogeneity corrosion

Since electrical and optical calcium corrosion tests do not directly monitor the corrosion of calcium, but instead monitor the effects of this corrosion on the conductance or the optical transmission of a calcium layer, relating conductance or optical transmission data to the amount of remaining metallic calcium, a model making this relation unique is required. Typically, this model is the lateral homogeneity of corrosion, i.e. the remaining metallic calcium film has a constant thickness over the whole layer during the course of the corrosion process. This homogeneous model is justified by a homogeneous distribution of the penetrant (water vapor) over the sample. This can

be ensured by using a glass cover with a cavity to distribute the permeating gas [48].

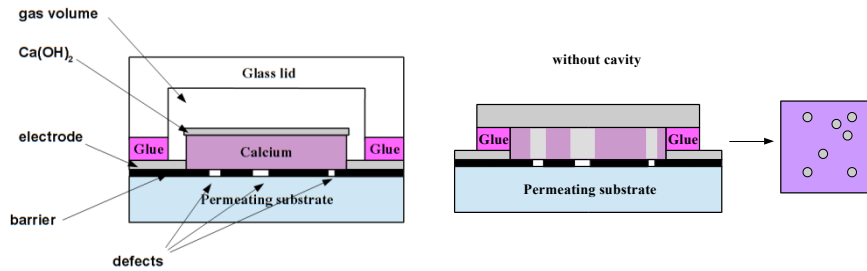


**Figure 3.1** - The gas volume allows water vapor to distribute and shall ensure for homogeneous corrosion.

Using all these information Calcium test sensors have been realized depositing by thermal evaporation first a Calcium layer with initial thickness of 100 nm and then the four Silver contact with initial thickness of 60 nm through shadow masks on glass substrate as showed in Figure 3.2.

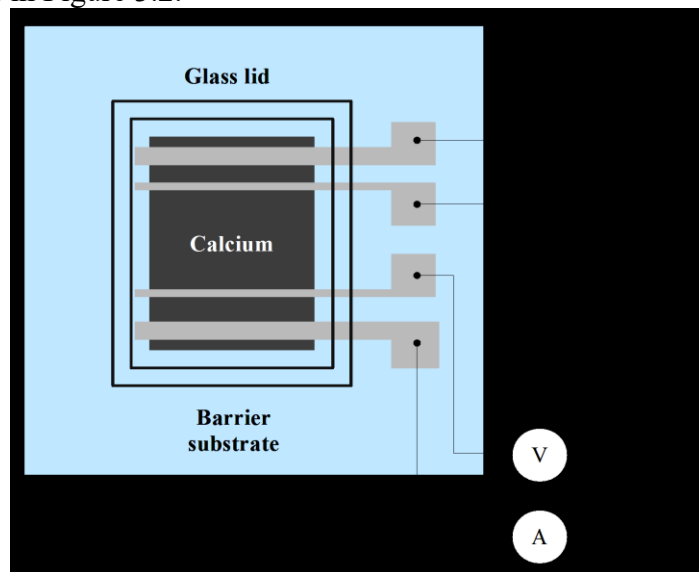


**Figure 3.2** - Schematic of the designed layout for electrical corrosion Calcium test measurement system

The Calcium thickness has been chosen in order to leave this layout suitable for both Electrical and Optical Calcium Test.

### 3.3 Measurement setup

The measurement setup for calcium tests was designed and improved at ENEA Portici. It is depicted in Figure 3.3 and consists of PC running control software, a Keithley2400 SourceMeter for the 4-wire-measurement of the conductance, a proper measurement station that accommodates the sample perfectly fitting the layout.

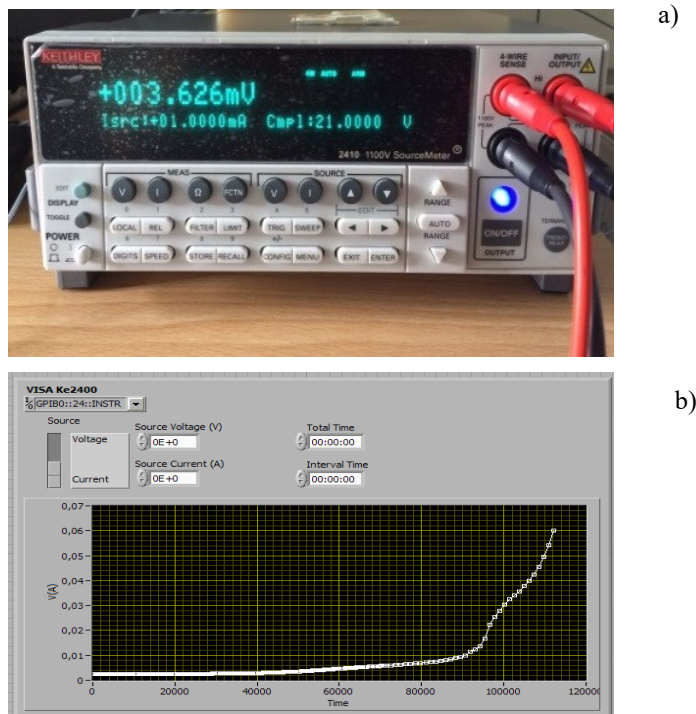


**Figure 3.3** - Keithley2400 SourceMeter a) and the control software developed for the automatic measure b)

In addition has been also used the Vötsch VC<sup>3</sup> 4018 climate chamber (Figure 3.4) that allows controlling temperature and humidity values. Temperature variation, range from 10 °C to 90 °C while the humidity can be regulated from 10 % to 98%.

These features allow measurements at different conditions, useful to perform accelerate test and to better analyze barrier quality.



**Figure 3.4** - Votsch climate chamber utilized for Electrical Calcium Test conditionings and measurement station for accommodation of the sample

### 3.4 Sample realization

Both metals used for sensor realization were deposited through an Ultra High Vacuum (UHV) thermal evaporation system produced by Kurt J. Lesker Company based on Super-SPECTROS 200 evaporator. The whole equipment was incorporated in a Jacomex glove box (Figure 3.5) and installed inside a class 100 clean room.



**Figure 3.5** - Kurt J. Lesker Company evaporator system incorporated in a Jacomex glove box used for metal evaporations

Metal to be evaporated are contained in suitable "container" known as *boat* and heated through an electrical system. The desired geometry has been obtained with two stainless steel shadow masks properly designed for this work. The sensor has been realized on glass substrate evaporating first a 90 nm thin layer of Calcium and then a 100 nm thin film of Silver. After evaporation, the samples were transferred to another glovebox containing a UV-lamp as well as a Nordson EFD dispenser for automatic dispensing of the glue (Figure 3.6).

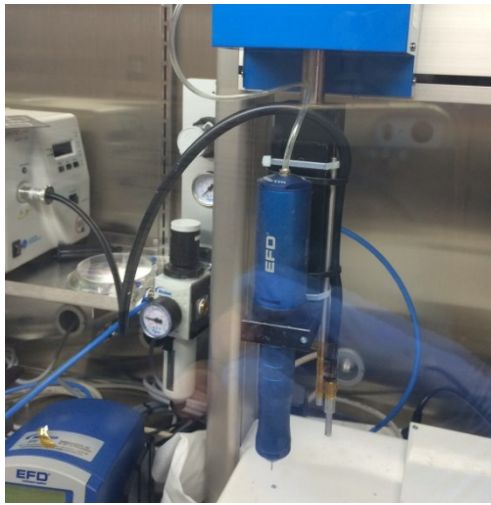


**Figure 3.6** - Nordson EFD automatic dispenser used for resin dispensation included in an MBRAUN glove box

To encapsulate a sample with a cavity glass, glue was automatically applied to the glass substrate and the cavity glass was then pressed onto the sample, making the lid perimeter perfectly overlap with the glue. The positioning of the cavity glass was made manually through a vacuum pen. The UV-curing process has been made connecting an optical fiber to the automatic dispenser. In this way only the glue rim has been exposed to the UV radiation.

### 3.5 Evaluation of measurement curves and WVTR calculation

According to the most widely used model [49] for the analysis of measurement curves and WVTR calculation and with regard to a constant WVTR, the measurement curve of the electrical calcium test (current vs. time) should exhibit a constant slope. Hence, the WVTR could be calculated using the following equation:

$$WVTR = -2 \frac{m_{H_2O}}{m_{Ca}} \delta_{Ca} \rho_{Ca} \frac{L}{W} \frac{d}{dt} \left( \frac{1}{R} \right) \quad (3.1)$$

where:  $m_{H_2O}$  and  $m_{Ca}$  are the molar masses of water vapor (18.0153 g mol<sup>-1</sup>) and Ca (40.08 g mol<sup>-1</sup>) respectively,  $\delta_{Ca}$  and  $\rho_{Ca}$  are the density (1.55 g cm<sup>-3</sup>) and the resistivity (3.4 10<sup>-8</sup> Ω m) of the initial metallic Ca respectively and are supposed to be constant, L and W are the length and width of the Ca pad and 1/R is the slope of the linear part of the conductance curve plotted versus measurement time t.

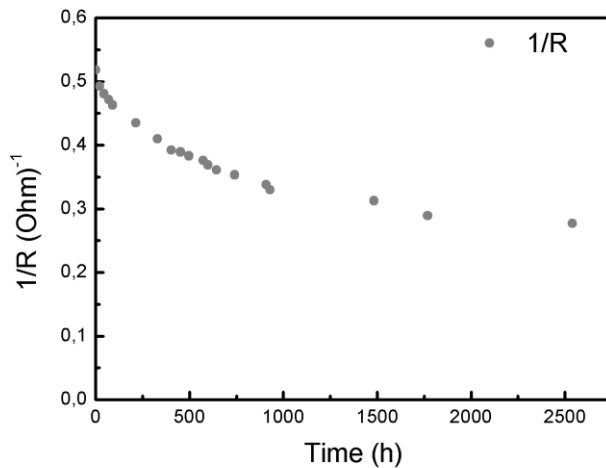


**Figure 3.7** - Conductance curve versus time for encapsulated 100 nm thick Ca pad measured at 25°C and 90%RH.

The previous expression is valid in the case of glass to glass system where the permeating surface is represented only by the glue rim. WVTR of barrier substrates to be studied can be evaluated instead, according to the following equation:

$$WVTR = -2 \frac{m_{H_2O}}{m_{Ca}} \delta_{Ca} \rho_{Ca} \frac{L}{W} \frac{A_{Ca}}{A_{window}} \frac{d}{dt} \left( \frac{1}{R} \right) \quad (3.2)$$

where all the parameters are the same as above quoted, with the exception of  $A_{window}$  that is the area of the encapsulated barrier layer. Even if these are the most used models, there are many assumptions contained in this theory, such as:

- the corrosion is homogeneous in a lateral direction.
- all incoming water instantaneously reacts with the calcium, meaning that there is no adsorption at inner walls or deceleration due to reaction kinetics
- the temperature, and thus the resistivity and the permeation, remains constant.
- the barrier is not damaged by the calcium test, i.e. there is no damage caused by corroding calcium.

Not all of those assumptions may be appropriate for any given measurement. Thus, those ideal curves are far from being usual for every barrier. So it is very important to analyze and interpret carefully the curve to identify the linear zone that corresponds to a constant WVTR.

### **3.6 Limitation and future perspective of Electrical Calcium Test**

The detection limit of electrical calcium tests, in principle, depends only on the quality of the perimeter sealing. This value has to be preliminarily measured by exposing it to different environmental conditions and represents the background for each condition. In fact, in order to properly evaluate the degradation of the calcium deposited on a barrier substrate and encapsulated with glass by sealing resin, the permeation through the sealing must be at least 10 times lower than that of the barrier layer of which the measurement is being carried out [50], since the total flux permeating is the sum of the flows permeating through the substrate plus that through the resin.

Also time, due to practical reasons, could be a limiting factor as well. Suppose the upper limit for measurement time is fixed in 100 days and 1 nm of calcium to be the minimum recognizable thickness change. Since  $1.4 \cdot 10^{-3} \text{ g(H}_2\text{O) m}^{-2}$  are required to corrode 1 nm of calcium and using a calcium area as large as the permeation barrier under test, the detection limit is in the range of  $10^{-5} \text{ g(H}_2\text{O) m}^{-2} \text{ day}^{-1}$ .

Anyway, by a better detection limit for the calcium thickness or by using a calcium area much smaller than the area of the barrier under test [51], the sensitivity can be further improved.

The sensitivity can be also enhanced improving the quality of the sealing to upgrade the background. Recently the trend is to choose an epoxy based resin with dehydrating agent added. This expedient

### 3.6 – Limitation and future perspective of Electrical Calcium Test 61

allows to have better performances and makes the system more sensitive.

In addition, there is still the opportunity to accelerate the measurement by elevated temperatures or humidity and, in consequence, yield a higher sensitivity due to re-calculation to moderate conditions.

## **Chapter 4**

# **4 Development of a glass to glass encapsulation system**

As shown previously, glass to glass approach is the best solution for devices realized on glass substrate. Thus it results very important to realize highly performant glass to glass encapsulation system. In addition this kind of system represents the background for the Electrical Calcium Test measurement system; so the most performing the encapsulation system is the most sensitive the measurement system become. This chapter is focused on the design, realization and optimization of a highly performing glass to glass encapsulation system.

## **4.1 Layout choice**

During the development of an encapsulation system the first issue to face is how to make the device terminals available for the contact. In order to make this possible a careful design of the encapsulation layout is requested. Our layout has been designed at ENEA Portici and uses a double contact between the device terminal and the two terminals available for the contact outside the encapsulation volume.

In Figure 4.1 and 4.2 are presented two layouts under ENEA Patent (Patent US 2009/0066244 A1: Tassini P., et al., “Encapsulated organic electronic device with improved resistance to degradation”, 12/03/2009; TO2007U000116: Tassini P., et al., “Dispositivo elettronico organico incapsulato, con migliorata resistenza al degrado”, 11/09/2007). The first shows a rectangular emissive area of

1cm<sup>2</sup> while the second has been studied to encapsulate three devices with one lid and every single devices shows a round active area of 0.071 cm<sup>2</sup> (3 mm diameter).

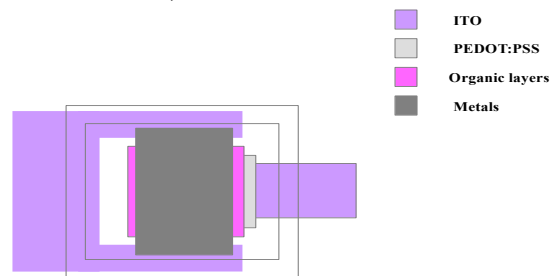


**Figure 4.1** - OLEDs encapsulation layouts with rectangular emitting area of 1 cm<sup>2</sup> while the glass lid used for the encapsulation

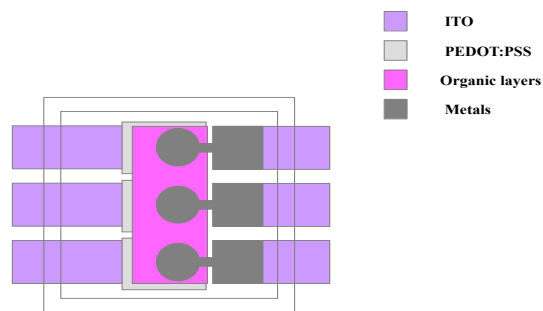


**Figure 4.2** - OLEDs encapsulation layouts studied for the encapsulation of three devices with 0.07 cm<sup>2</sup> round area simultaneously

The first layout has been chosen because it has the same Calcium area of our Calcium test sensor. This characteristic would make possible a direct correlation between Calcium degradation evaluated for a Calcium test sensor and OLED device degradation.

## 4.2 Encapsulation process parameters optimization

Dealing with glass to glass encapsulation the permeating surface is entirely represented by the sealing rim. Thus in order to improve the

system performances it is very important to optimize sealing geometry as though its physical and chemical characteristics.

First we focus on the total volume of dispensed resin to reduce the total permeating surface. Different tests have been made, using several weights for different times to find out the optimal pressure of lamination value to maximize the diffusion path. Every sample has been characterized in terms of thickness. Starting from a 450  $\mu\text{m}$  value it has been reached a thickness of 100  $\mu\text{m}$  using a 15 g weight for 20 seconds.

This geometry allows the resin to cover entirely and homogeneously the lid frame; in this way it has been possible to have a thin, smooth and uniform glue rim. Then it has been accurately selected the sealing glue. It has been chosen the epoxy based resin Zeogluce produced by SAES getter. This glue showed excellent sealing property, also thanks to its formula with the addition of zeolite particles that have moisture adsorbing properties, and very good adhesion.

The resin has been dispensed through the automatic dispenser Nordson EFD following the encapsulation layout. The glass lid has been positioned manually using a vacuum pen also used for the positioning of the weight.

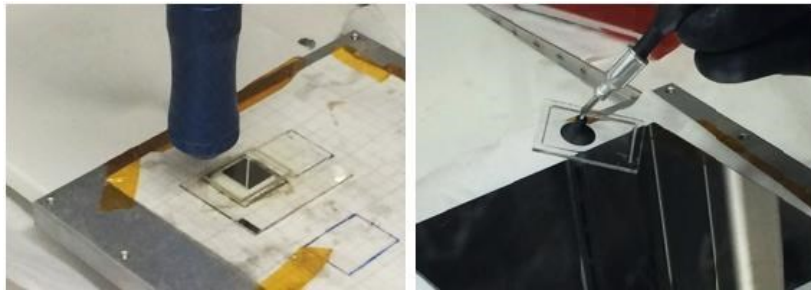


**Figure 4.3** - On the left the glue dispensation through Nordson EFD dispenser while on the right the glass lid positioning

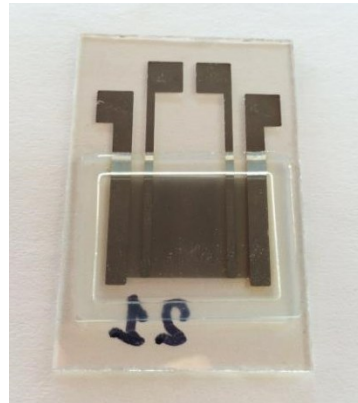


**Figure 4.4** - Encapsulated sample with a optimized coverage of the lid frame

Later we focused on the curing process parameters. First it has been chosen a UV lamp able to supply the resin desired wavelength. It has been chosen the UV Lamp Omnicure S2000 with wavelength of 365 nm coupled with an optic fiber of 3mm diameter. Then using the maximum energy density for the correct resin curing process that is  $12 \text{ J cm}^{-2}$  and using the fact that the energy density is the product between the power density (lamp irradiation) and the time (curing time) it has been identified various couples of value for the irradiance and the time that perfectly match the sealing requirements.

In order to adjust the UV lamp irradiance value it has also been used a radiometer choosing the maximum lamp irradiation value of  $1000 \text{ mW cm}^{-2}$ .

Using this value from the previous relation has been identified the curing process time of 12 seconds. At this point, different tests have been made to decide the UV-curing process speed for the optical fiber movement. This value resulted extremely important to increase the crosslink density of the resin. First some test has been made with high speed passing multiple times on the same section of glue rim perimeter. Then, since the UV radiation shows a reduced penetration length, the best results, in terms of adhesion and resin degradation, has been reached using the slowest speed and passing just once on every section. Using the fact that the spot of optical fiber has a 3mm section the desired speed can be found by:

$$v = \frac{3\text{mm}}{12\text{s}} = 0,25 \frac{\text{mm}}{\text{sec}} \quad (4.1)$$

In order to assure the complete curing process the selected speed for UV curing process is reduced to  $0.2 \text{ mm sec}^{-1}$ . Finally the curing process has been realized with an optic fiber connected to the UV lamp (Figure 4.5).

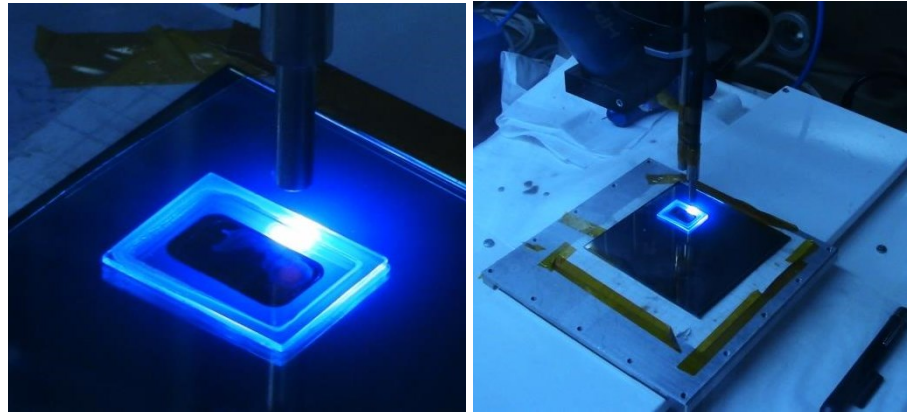


**Figure 4.5** - The UV curing process realized with an optic fiber connected to the UV lamp.

Using all the optimized parameters it has been defined a glass to glass encapsulation process for the encapsulation of devices realized on glass or rigid substrate. In following section the results about the characterization of the optimized system will be presented. During the optimization process, Electrical Calcium Test has been also used to evaluate system performances.

### **4.3 Encapsulation characterization through Electrical Calcium Test**

The glass to glass encapsulation system described in the previous section has been here characterized using the Electrical Calcium Test presented in the preceding chapter.

Sensors realization

A Calcium sensor with Aluminum contact has been evaporated on glass substrate using the UHV Kurt J. Lesker system. Immediately after fabrication the samples have been encapsulated with our optimized procedure into a glove box with controlled level of oxygen and humidity.

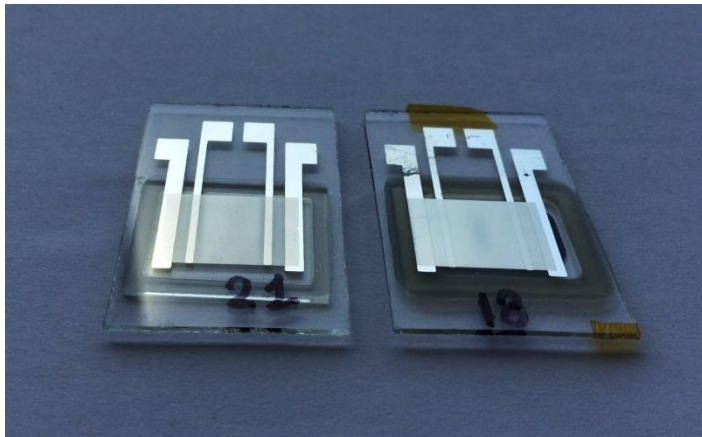


**Figure 4.6** - Sample realized for the characterization through Electrical Calcium Test of glass to glass encapsulation system

It has been also realized some devices introducing into the sealed volume a dehydrating agent known as getter. Typical getters are based on thin film of CaO. Schematic of the glass to glass encapsulation system with the addition of getter is shown in Figure 4.7.

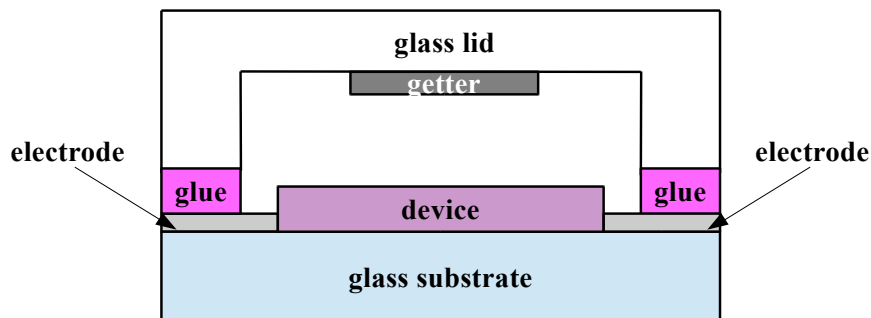


**Figure 4.7** - Schematic of a glass to glass encapsulation system with a getter into the sealed volume

After some tests we choose the Dryflex produced by SAES Getter. It is a thin adhesive getter that has been glued under the lid.

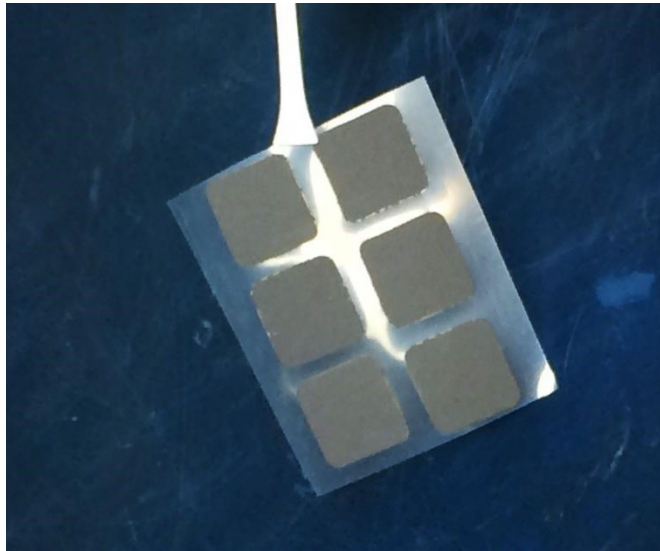


**Figure 4.8** - Thin adhesive getter Dryflex produced by SAES Getter

### **4.3.1 Calcium Test results at ambient condition**

Both types of samples have been kept at 25°C and 50 RH, realized in a climate chamber. The conductance has been evaluated periodically. In Figure 4.9 and 4.10, conductance vs time curves from two of the realized samples respectively without and with getter are shown.

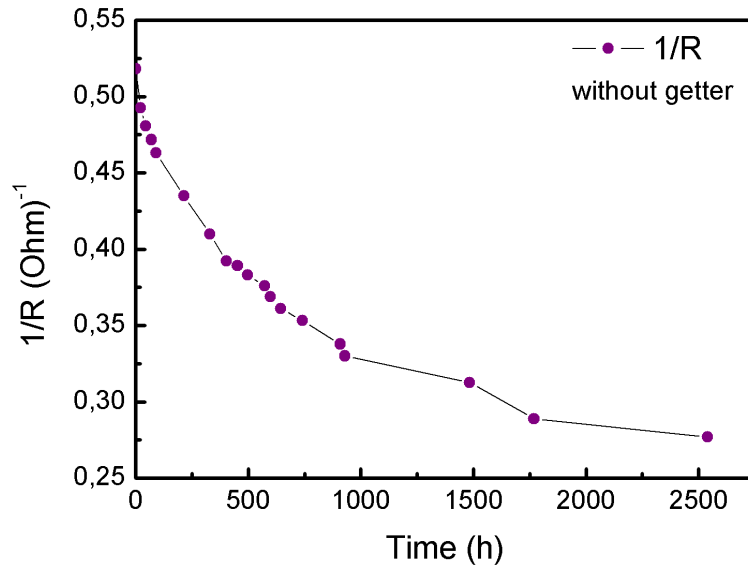


Figure 4.9 - Conductance versus time curves for a Calcium sample without getter in the sealed volume

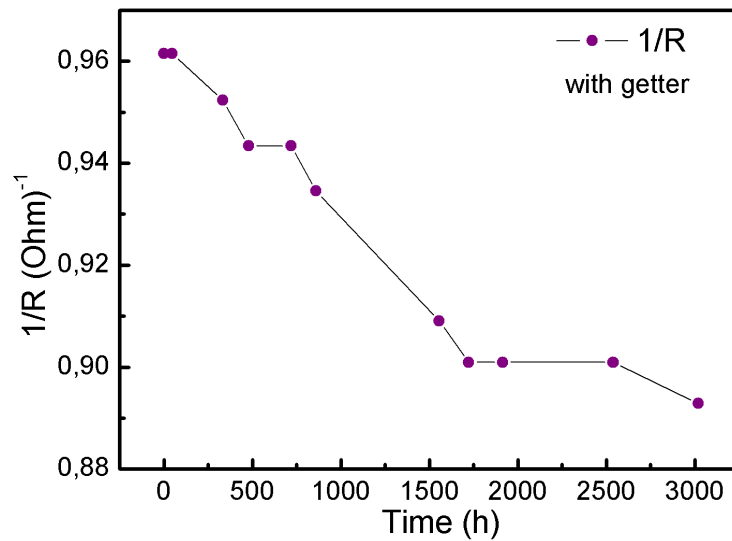


Figure 4.10 - Conductance versus time curves for a Calcium sample with getter in the sealed volume

From these curves, WVTR values of  $4 \cdot 10^{-5} \text{ g m}^{-2} \text{ day}^{-1}$  and of  $4 \cdot 10^{-6} \text{ g m}^{-2} \text{ day}^{-1}$  were derived. These results are extremely positive since they are in line with literature results obtained with glass to glass approach. Furthermore, since these values represent the background for flexible Calcium test measurement, these results are very encouraging also for flexible encapsulation system developing and characterizing.

### **4.3.2 Calcium Test results for various conditioning**

Thanks to the climate chamber it has been also possible to perform measures at different conditioning. The results for a sample without getter are showed in Table 4.1.

Conditioning	WVTR ( $\text{g m}^{-2} \text{ day}^{-1}$ )
25°C, 50 RH	$2.9 \cdot 10^{-5}$
38°C, 90 RH	$8.9 \cdot 10^{-4}$
65°C, 85 RH	$7.8 \cdot 10^{-3}$

**Table 4.1** - Temperature and humidity conditions and relative WVTR values derived for the glass to glass encapsulation system

## **4.4 Validation of the encapsulation system through device degradation in accelerated atmosphere**

In order to validate the results obtained through Electrical Calcium test, OLED devices have been realized and then encapsulated with our system. The devices layout is represented in figure 4.11.

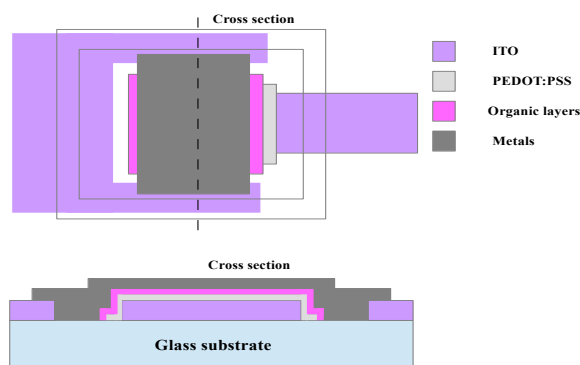


**Figure 4.11** - OLEDs layout used for the validation samples. Dashed line identifies the cross section.

In this part of the work a simple OLED structure was employed as validation device. In figure 4.12 and 4.13 energy levels and structure layers are illustrated. The stack consists of ITO as bottom electrode, a 35 nm thick hole injection layer of PEDOT:pss, a 40 nm thick hole-transporting layer of NPD (N,N'-bis(1-naphthyl)-N,N'-diphenyl-1,1'-biphenyl-4,4'-diamine), a 60 nm thick emitter layer of Alq<sub>3</sub> (Tris (8-hydroxyquinolinato) aluminium), followed by a 20 nm thick layer of Calcium and finally a 80 nm thick top electrode of Aluminum.

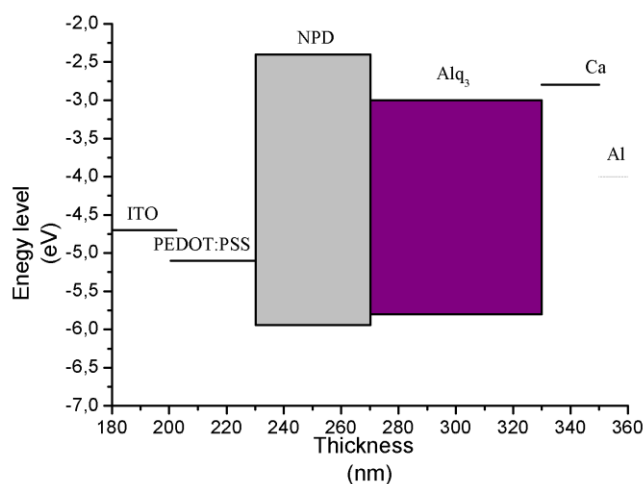


**Figure 4.12** - Structure and energy levels for the device with Alq<sub>3</sub> as emitter layer

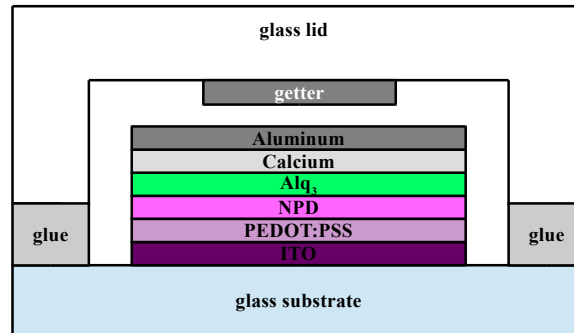


**Figure 4.13** - Schematic of the structure of the encapsulated device

After the realization the devices have been immediately encapsulated and then initial electrical and optical characteristics were measured using respectively a Keithley 2400 SourceMeter and a Gooch&Housego OL770 spectroradiometer coupled with an integrating sphere and a camera telescope. The devices were then stored for extended periods at 38 °C and 90 RH and periodically measured in terms of electrical and optical characteristics. In Figure 4.14 has been reported the realized devices spectrum; from the curve it is easily to recognize the typical peak of Alq<sub>3</sub> emitter. In the inset one of the realized devices is showed under polarization while in Figure 4.15 and 4.16 the luminance vs time for two devices, one without and one employing a getter is depicted.

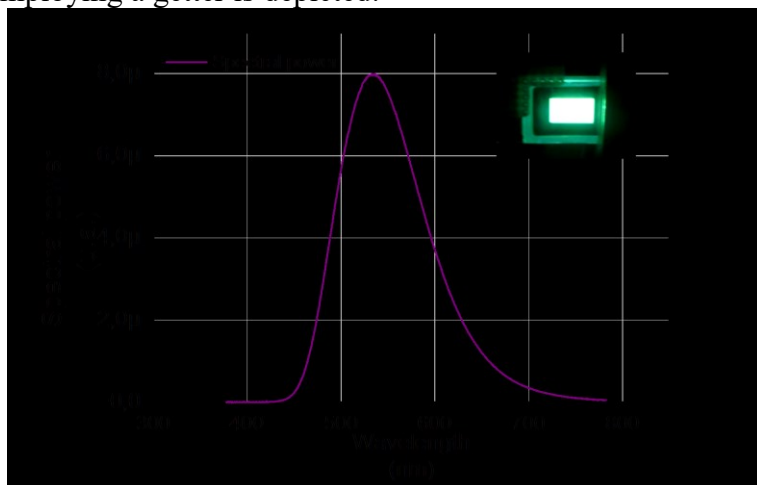


**Figure 4.14** - Spectral power of the realized devices. In the inset it has been reported one of the devices under operation.

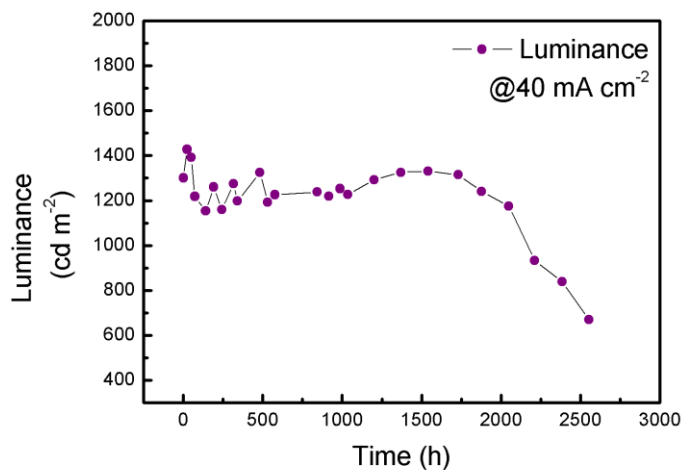


Figure 4.15 - Luminance vs time curve @ 40 mA cm<sup>-2</sup> for the device without getter

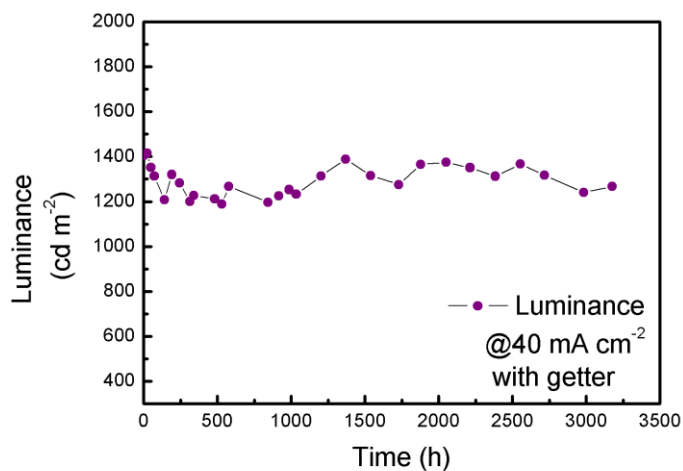


Figure 4.16 - Luminance vs time curve @ 40 mA cm<sup>-2</sup> for the device with getter

The devices encapsulated with the described system, with and without getter, did not lose more than 20% of the initial luminescence value after approximately 3000 hours.

These results showed the efficacy of the developed encapsulation system that thanks to this property makes possible to neglect the

74 Chapter 4 - Development of a glass to glass encapsulation system

influence of external degradation phenomena within the analyzed time window. This opportunity represents the fundamental basis for studying intrinsic degradation

## **Chapter 5**

# **5 Development of a flexible barrier layer encapsulation system**

The environmental stability of the organic electronic devices remains one of the most important limits for their broad commercialization. Encapsulation of the devices is thus required to achieve adequate lifetime. Especially in the case of flexible substrates, this issue represents still a challenge, [52]. Several flexible encapsulation approaches have been proposed in the recent years as has been described in section 2.4. In this chapter it is described the choice of Thin Film Encapsulation approach and the design and development of our flexible encapsulation system.

## **5.1 Thin Film Encapsulation choice**

Among all the flexible encapsulation approaches, it has been selected the Thin Film Encapsulation (TFE) approach because it is preferable having a thinner-lighter form factor and a higher flexibility, minimizing the mechanical stress and abrasion to the barrier that is positioned as close as possible to the sensitive layers and being ideally used into roll-to-roll manufacturing, reducing the number of the process steps and costs [30] [13]; moreover, TFE can be combined with other low-cost encapsulation technologies, such as roll-to-roll lamination. However, any contact to the device by adverse agents (i.e. solvents) must be minimized and the process must be performed at relatively low temperatures. Therefore, many technologies involving high temperatures to achieve dense inorganic barrier layers cannot be

employed in TFE processes. Typical TFE involves the deposition of inorganic barrier layers, mainly oxides, on the substrate or directly on the device from vacuum deposition techniques (sputtering, ALD, PECVD, e-beam evaporation).

Based on all these premises, it has been studied and realized a flexible multilayer barrier structure, selecting the TFE method, realizing inorganic-organic multilayer barrier stack based on sputtered Al<sub>2</sub>O<sub>3</sub> layers, as described in the following sections.

## **5.2 Developing and optimizing of single thin inorganic Al<sub>2</sub>O<sub>3</sub> layer for multilayer barrier structure**

As single inorganic layer deposition technology, sputtering was used since permeation barrier properties superior to evaporated layers can be achieved [13]. As inorganic barrier layer, Al<sub>2</sub>O<sub>3</sub> was used because has very dense structure and the lowest water vapor transmission rate of all sputtered inorganic layers [13]; moreover, very low surface roughness of Al<sub>2</sub>O<sub>3</sub> can be achieved by sputtering. Regarding the sputtering technique, non-reactive RF one was chosen to be used, since better barrier performance can be achieved despite a slower rate deposition [53] [54].

In order to study the barrier performance of the inorganic layer, Al<sub>2</sub>O<sub>3</sub> was sputtered onto the chemically pretreated side (for the adhesion improvement) of a 125 μm thick flexible PEN substrate (DuPont Teijin Films/Teonex® Q65FA) using a Kurt J. Lesker Company Spectros® system (Figure 5.1). The used PEN also has a very smooth surface (average of 13 nm) and was chosen because of its better thermal and mechanical properties compared to other polymers such as PET.

Preliminary Al<sub>2</sub>O<sub>3</sub> sputtering tests were performed on PEN, varying the flow of the argon at fixed power of 140 W (maximum

power that can be used, as indicated by the manufacturer of the used sputtering system). In this way, through the optical profilometer measurements, it was possible to obtain for the different flows, the related rate of deposition of Al<sub>2</sub>O<sub>3</sub> (measuring the thickness of the deposited layers) and directly evaluate the surface roughness of the deposited layers (Table 5.1).

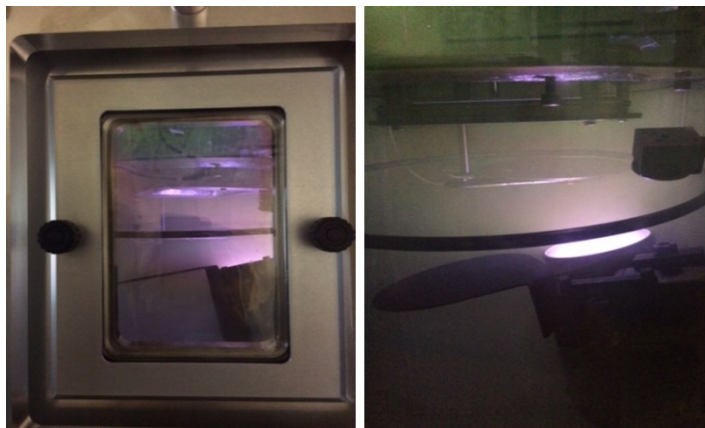


**Figure 5.1** - Plasma discharge in Argon in the Kurt J. Lesker sputtering system used for RF sputtering deposition of Al<sub>2</sub>O<sub>3</sub>.

Ar flow (sccm)	Rate of deposition (Å/s)	Avarage surface roughness (nm)
10	0,17	5
20	0,32	9
30	0,09	11

**Table 5.1** - Rate of deposition and surface roughness obtained for depositing Al<sub>2</sub>O<sub>3</sub> on PEN substrate by non-reactive sputtering at different argon flows.

So, discarding the higher flow (30 sccm), in order to assess the quality of the deposition processes, it was decided to perform water vapor permeability tests by using a commercial permeabilimeter PermeoH<sub>2</sub>O by ExtraSolution, (Figure 5.2) of 120 nm thick Al<sub>2</sub>O<sub>3</sub> layers deposited on PEN at 10 and 20 sccm of Ar (Figure 5.3). As it can be seen, at the same thickness of deposited Al<sub>2</sub>O<sub>3</sub>, the reduced flow of argon

generates a better quality (lower defects) of the inorganic layer (also highlighted by the low surface roughness obtained), halving the permeability.



**Figure 5.2** - PermeoH<sub>2</sub>O permeabilimeter by ExtraSolution for WVTR barrier film measurement.

On the basis of what was obtained, a scan varying the thickness of deposited Al<sub>2</sub>O<sub>3</sub> with optimized recipe (140W, 10 sccm of Ar) was then carried out. As from Figure 5.4., the thickness of 210 nm exhibited the maximum value of barrier (WVTR of 0.07 g m<sup>-2</sup> day<sup>-1</sup> at 38°C and 90% RH) achievable from a deposited single layer of the inorganic material; higher thicknesses did not result in further improvements. Such result constitutes the basis for the realization of multilayer inorganic-organic structures to obtain higher barrier values.

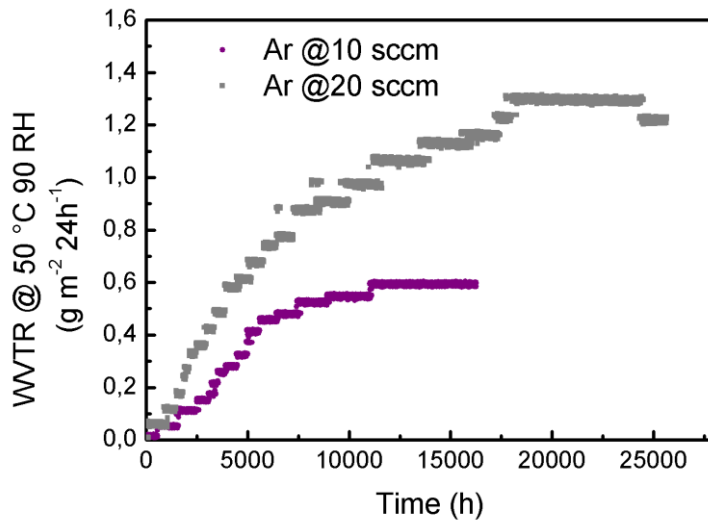


Figure 5.3 - WVTRs @ 50°C and 90%RH of PEN with Al<sub>2</sub>O<sub>3</sub> at fixed thickness (120 nm) deposited with different Ar flow.

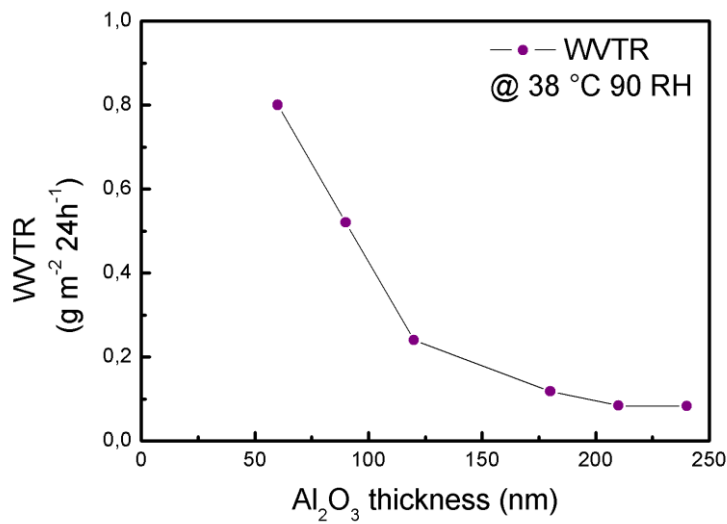


Figure 5.4 - WVTRs @ 38°C and 90%RH of PEN samples coated with Al<sub>2</sub>O<sub>3</sub> of different thicknesses.

### **5.3 Developing and optimizing of organic intralayer for multilayer barrier structure**

Once optimized the sputtering of  $\text{Al}_2\text{O}_3$ , the identification of possible polymeric materials suitable to be used as organic inter-layer in multilayer barrier structures was carried out.

As reported in literature, the use of polymers deposited from a liquid phase is to be preferable, since their good wettability on the surface of the inorganic allows its complete coverage and of its defects [13]. Therefore, some different commercial coatings were selected to test adopted from printed packaging industry, suitable to be printed on the inorganic layer and having high temperature resistance and good flatness.

As deposition method, printing was adopted as low-cost and roll-to-roll compatible technique. These products were printed on flexible PEN by means of a K-bar and compared in terms of adhesion and surface roughness at the same printing conditions and solid content. From the comparison, a polyurethane based coating was selected showing the lowest surface roughness.

Then, to further reduce its surface roughness, other tests were made by varying process conditions and its dilution; in particular, the coating was first diluted by adding 50 and 100wt% of solvent (ethyl acetate). The most diluted sample (Figure 5.5 b) presented a lower roughness; in order to further reduce it, a post-treatment by printing only solvent on the surface of the latter sample (Figure 5.5 c) was then carried out, achieving an additional improvement (Table 5.2). But, in order to maximize the barrier performance of the multilayer structure to be realized, it was considered to further improve the characteristics of the organic layer in terms of reduction of thickness (to increase the diffusive path between defects of successive inorganic barrier layers) and of surface roughness (maximizing the barrier effect of the inorganic layer subsequently deposited on it).

Therefore, other tests were carried out, adding more solvent and varying the conditions of the printing process: since the solvent content is high, different timing and type of drying have been tried, in

order to avoid possible cracking phenomena on the surface of the underlying inorganic layer, due to an excessive evaporation of extremely volatile solvent. From tests, the coating printed by adding 150wt% of solvent and dried slowly for one hour in Petri dish gave better results (Figure 5.5 d and Table 5.2).

	Sample	Surface roughness (nm)	Organic thickness (nm)
a	Organic coating diluted with 50wt% of solvent	54	940
b	Organic coating diluted with 100wt% of solvent	35	620
c	Organic coating diluted with 100wt% of solvent + solvent post-treatment	26	480
d	Organic coating diluted with 150wt% of solvent + slow drying	13	410

**Table 5.2** - Surface roughness and thickness of organic coating printed with different conditions.

In particular, the surface roughness is really low and similar to that obtained for the inorganic layer previously optimized (about 7 nm). This optimized process was therefore used to deposit the organic interlayer of the multilayer barrier structure as the next section.

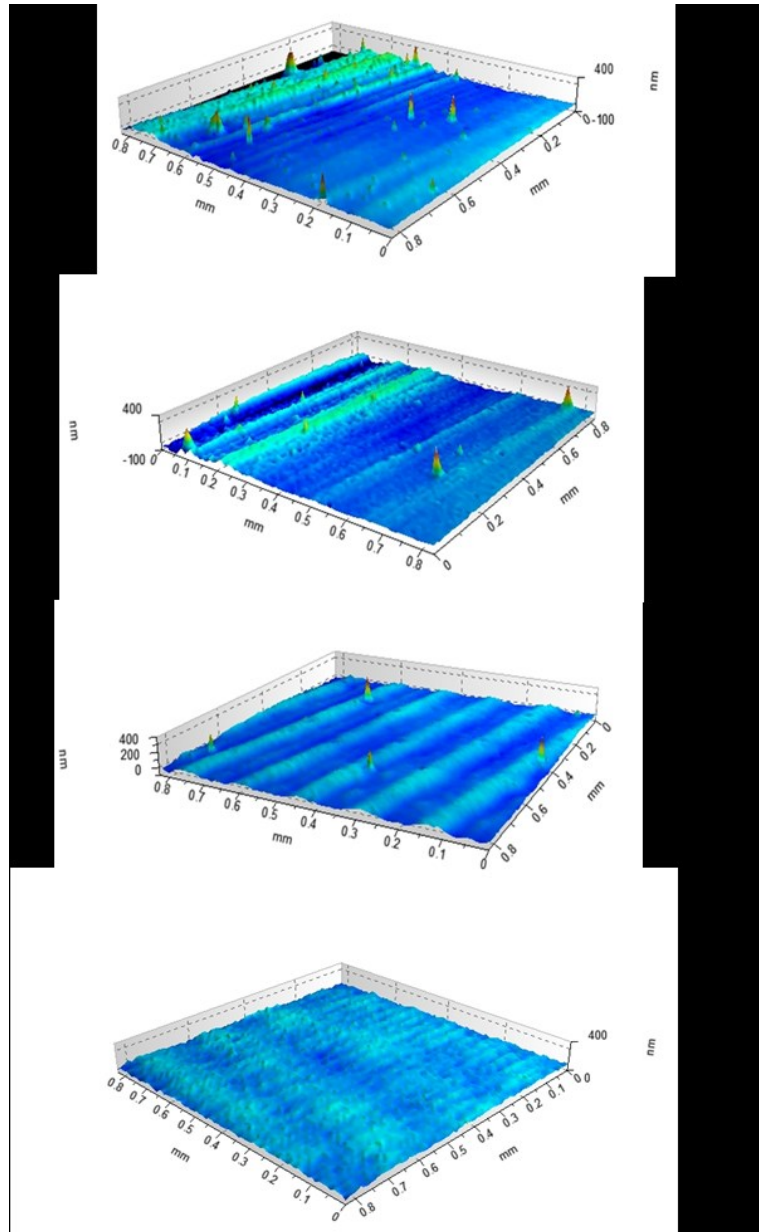


**Figure 5.5** - Morphological surface of PEN samples printed with: a) organic coating diluted with 50wt% of solvent; b) organic coating diluted with 100wt% of solvent; c) organic coating diluted with 100wt% of solvent + solvent post-treatment; d) organic coating diluted with 150wt% of solvent + slow drying (1h in Petri).

## 5.4 Making multilayer inorganic-organic barrier structure on flexible PEN substrate

On the basis of the optimization of the processes for the deposition of the single inorganic and organic layers, multilayer barrier structures consisted of 3 dyads (pairs of layers of inorganic-organic) on PEN were realized (Figure 5.6).

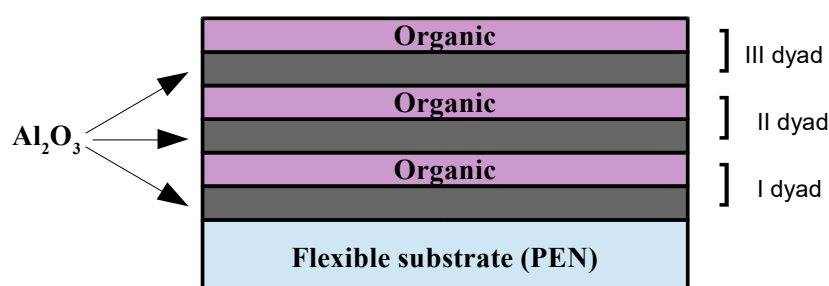
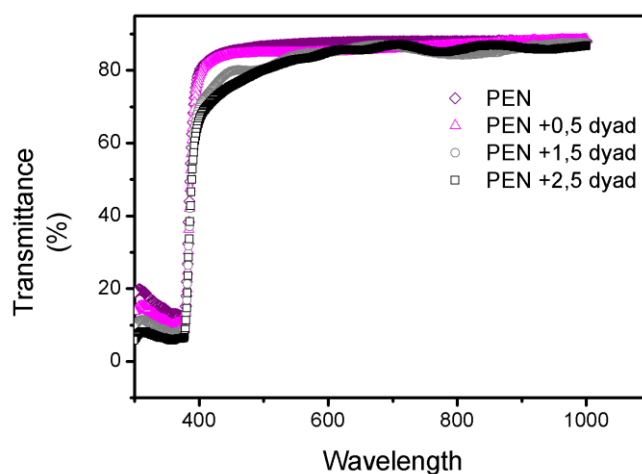


Figure 5.6 - Schematic of realized multilayer barrier structure.

An optical transmittance over 80% was also obtained by such multilayers as showed in Figure 5.7; the difference in the spectra is clearly due to the different thickness generated by the number of the overlapped layers.

The barrier performance of these samples was evaluated by Electrical Calcium Test performed at 38°C and 90% RH condition, realized in a climate chamber. Calcium Test sample on PEN has been realized for the single pair (one dyad) of organic-inorganic barrier, for the doubled pair (two dyads) and for the 3dyads barrier layer.



**Figure 5.7** - UV-VIS-NIR transmittance measurements of multilayer barrier structure on PEN substrate with different number of dyads (pair of layers of  $\text{Al}_2\text{O}_3$ -organic).

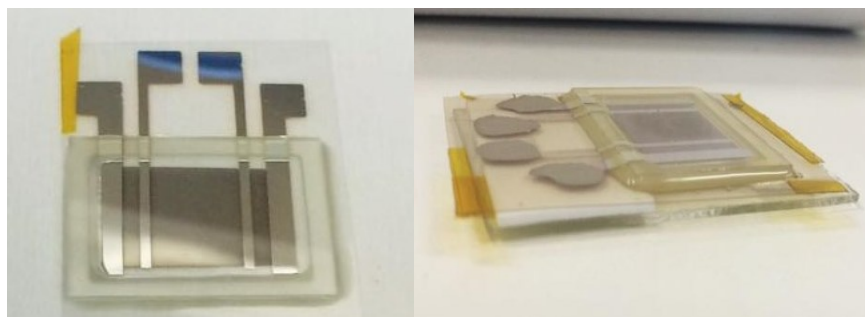


**Figure 5.8** – Sample on PEN realized for the evaluation through Electrical Calcium Test of multilayer barrier structure

Conductance vs time curves with increasing of the number of dyads are shown in Figure 5.9.

From these curves, WVTR values of Table 5.3 were derived. As it can be seen, the optimization of the deposition of both layers (inorganic and organic) and the adoption of more dyads allowed reducing the water vapor permeability of the structure reaching  $0.02 \text{ g m}^{-2} \text{ day}^{-1}$  for 3dyads sample. Because the permeability presents an Arrhenius-like trend, this value corresponds to about  $0.007 \text{ g m}^{-2} \text{ day}^{-1}$

at room conditions (25°C and 50% RH). More dyads did not result in further improvements, rather occurring mechanical cracking. The obtained results are comparable with those of the literature relatively to the same methods (thin film encapsulation), deposition techniques (non-reactive sputtering) and materials used ( $\text{Al}_2\text{O}_3$ ) [53] [54].

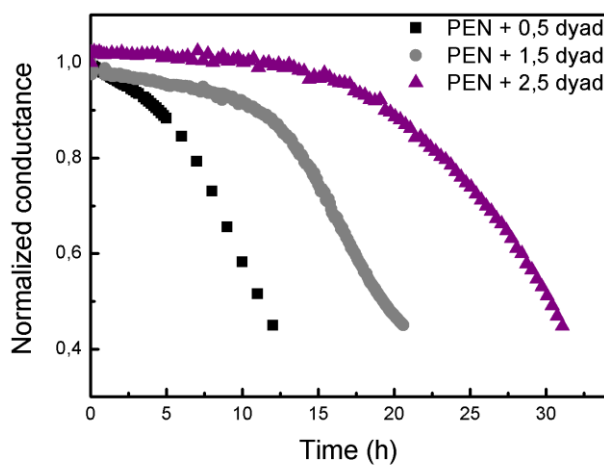


**Figure 5.9** - Conductance curves versus time (from electrical Ca test) at 38°C and 90%RH of multilayer barrier structure on PEN substrate with different number of dyads (pair of layers of  $\text{Al}_2\text{O}_3$ -organic).

Number of dyads ( $\text{Al}_2\text{O}_3$ -organic)	WVTR @38 °C 90 RH ( $\text{g m}^{-2} \text{day}^{-1}$ )	Lag time (h)
1	$6,7 \cdot 10^{-2}$	3,8
2	$5,1 \cdot 10^{-2}$	10,8
3	$2,2 \cdot 10^{-2}$	20,2

**Table 5.3** - WVTRs and lag times derived from electrical Ca test performed at 38°C and 90%RH of multilayer barrier structure on PEN substrate with different number of dyads (pair of layers of  $\text{Al}_2\text{O}_3$ -organic).

Although similar solutions with WVTR values much lower than those obtained by us are also presented in literatures, it must be said that very few of these results really represents equilibrium permeation. In fact, it has been showed that it is impossible to obtain an equilibrium water vapor permeation rates through multilayer barrier films  $< 10^{-4} \text{ g m}^{-2} \text{ day}^{-1}$  without very substantial reduction of the effective diffusivity

of the individual barrier layers [14]: multilayer series-resistance model predicts a minimal improvement in steady state flux that asymptotically approaches a lower value of  $10^{-2} \text{ g m}^{-2} \text{ day}^{-1}$  (as also obtained in this work) for structure from 1 up to 5 dyads involving  $\text{Al}_2\text{O}_3$  inorganic barrier layer from vacuum deposition techniques (with the exception of ALD).

However, it must be remarked the increase of the observed "lag time" with increasing of the number of dyads employed for the realization of the barrier structure. Such time delay is characteristic of the permeation process and it is a direct measure of the time required before reaching the steady state conditions (from which WVTR is calculated): namely, it indicates the transient in which the concentration profile of penetrating evolves within the barrier structure until reaching steady state conditions. So, an increasing of the lag time means a proportional increase in diffusive path of penetrating that takes more time to cross the barrier structure.

Therefore, the observed increase of the lag time indicates the validity of the adopted multi-layer solution, but also the good quality of the individual layers successively deposited: in fact, in case of deposited layers with a greater number of defects, no improvements would be observed with increasing of the layers, being valid the series-permeability of the structure. Even this observed increase is in line with the literature where, as suggested by calculations, a large increment of the lag time would extend device lifetimes regardless of the equilibrium permeability of the barrier layers [14]. In fact the device lifetime can be extended by both a lower steady state WVTR and a longer lag time [55].

## **Chapter 6**

### **6 Intrinsic degradation study**

As said for OLED, basically two types of degradation exist: extrinsic and intrinsic degradation [8]. As we saw before, the extrinsic degradation can be easily controlled by proper encapsulation. On the other hand understanding the origins of the intrinsic degradation remains a challenge and up to now. In addition the few proposed mechanisms, including: increase of the density of deep traps, morphological instability of holes transport layers, metal diffusion from the electrodes and photo-oxidation of organic layers by self-emitting light, [56] have not considered possible phenomena that can occur during OFF-time periods. In this chapter, intrinsic degradation phenomena have been studied through innovative shelf life experiments performed at different storage conditions on two types of blue OLEDs. Experiments revealed that physical aging occurs for both types of devices, leading to irreversible time-dependent luminance loss.

#### **6.1 New methodology for intrinsic degradation study**

In general, intrinsic degradation is monitored by means of accelerated degradation tests, typically performed by electrical stressing the device beyond its normal use, which permits lifetime estimation. A common lifetime metric is T50 value that corresponds to the time taken for the luminance to decay below 50% of its initial value under steady-state operation. However, such method does not consider

possible degradation phenomena that can anyway occur during OFF-time periods, namely when the device is not subjected to electrical stress.

Since extrinsic and intrinsic degradation are independent phenomena they can be considered as additive and consequently they can be studied separately under appropriate conditions. In the same fashion, it is possible to think about intrinsic degradation as the sum of different contributions, if the single mechanisms can be isolated with respect to the others. To this aim suitable experimental condition must be realized in order to neglect the influence of all the phenomena except from the one under analysis.

In this way OLED degradation can be described through the following equation:

$$\begin{aligned} \text{Degradation} = & \sum \text{Extrinsic degradation mechanisms} + \\ & \sum \text{Intrinsic degradation mechanisms} = E_1(WVTR) + \\ & E_2(OTR) + \dots + I_1(\text{morphological change}) + \\ & I_2(\text{metal diffusion}) + I_3(\text{chemical reaction}) + \dots \quad (5.1) \end{aligned}$$

This approach has been used in this work as an innovative method to study in detail intrinsic degradation problem.

More precisely, possible intrinsic degradation phenomena have been studied through shelf life experiments on, OLED devices, performed at different storage conditions. In order to minimize extrinsic degradation processes during the experimental time-frame of observation, devices have been encapsulated immediately after fabrication with the encapsulation system realized and characterized in the previous chapter. In this way it is possible to neglect the effect of external environment (water vapor, oxygen,...) and focus on the intrinsic degradation. Since the device have been characterized immediately after the realization and then periodically it is also possible to neglect electrical stress.

## 6.2 Case study: blue OLED devices

In order to demonstrate the validity of this innovative methodology it has been chosen to realize blue OLED. This type of devices has been selected because generally presents the worst stability respect to the other colors [57] [58]; this issue made their degradation extremely difficult to study.

### Sample preparation

Two types of devices have been realized: [59] structures and energy diagrams of the two types of blue OLEDs, using Phosphorescent (device A) and Fluorescent (device B) emitting materials, are illustrated respectively in Figure 6.1 and 6.2.

Devices were fabricated on commercial ITO-coated glass substrate opportunely patterned through photolithography and chemical etching (HCl solution based). Samples were washed in ultrasonic bath in deionized water with detergent at 80 °C for 1 hour, rinsed first in clean deionized water and then in isopropanol, and finally dried in an oven at 110 °C for 1 hour. as hole injection layer (HIL), water-diluted commercial PEDOT:PSS was spin coated in air on ITO and then dried in a vacuum oven (dry thickness 50 nm).

Functional organic layers and cathodes were deposited in a thermal evaporator, with base pressure lower than  $5 \cdot 10^{-7}$  mbar, through shadow mask at rates below  $1 \text{ \AA s}^{-1}$ . After fabrication, the samples underwent a thermal annealing for 1.5 h at 130 °C in vacuum. The emitting area of each device was fixed at about  $1 \text{ cm}^2$  and the layout was designed in order to keep the sensitive material entirely encapsulated.

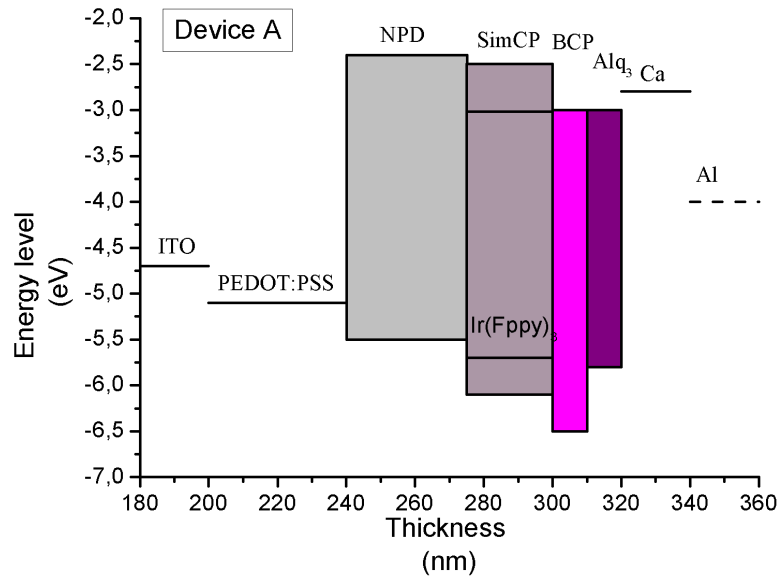


Figure 6.1 - Structure and energy levels for the Phosphorescent device (Device A)

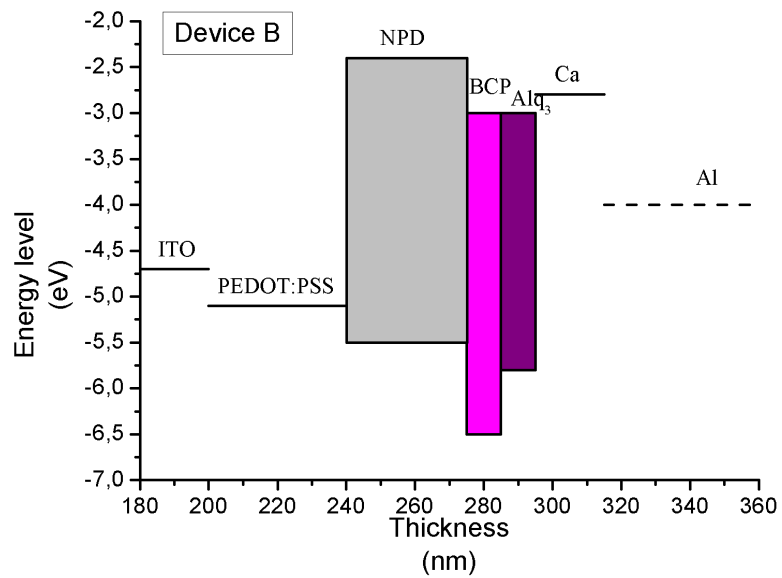
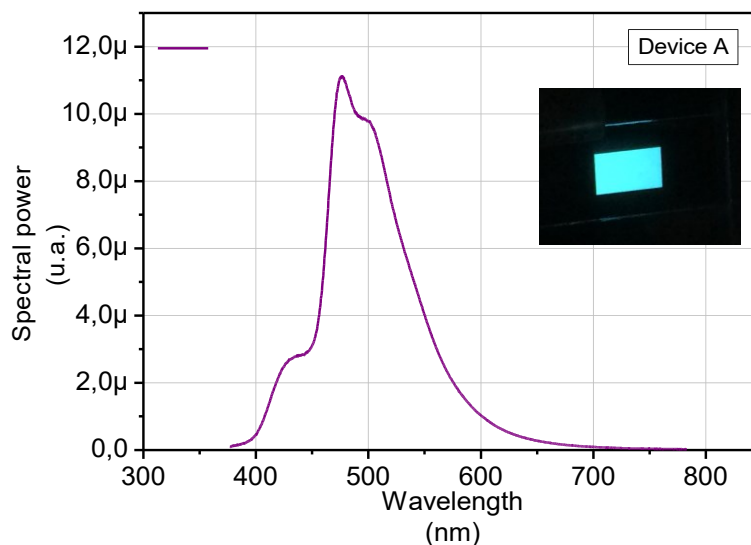


Figure 6.2 - Structure and energy levels for the Fluorescent device (Device B)

Devices were encapsulated immediately after fabrication inside a glove box, where oxygen and water are constantly kept under 1 ppm, fully covering them using our encapsulation system. The encapsulated devices were then stored for extended periods at the following conditions: a) 25°C, 0% RH; b) 25°C, 45% RH; c) 65°C, 0% RH.

Electrical and optical characteristics were periodically measured on the encapsulated devices using respectively a Keithley 2400 SourceMeter and a Gooch&Housego OL770 spectroradiometer coupled with an integrating sphere and a camera telescope; for each sampling, total luminous flux was collected at different current values (10, 20, 30 and 40 mA).

Spectral power are reported respectively for Phosphorescent (Device A) and Fluorescent (Device B) devices in figure 6.3 and 6.4 while in the insets are showed the realized devices under polarization.



**Figure 6.3** - Structure and energy levels for the Phosphorescent device (Device A); in the inset the device under operation

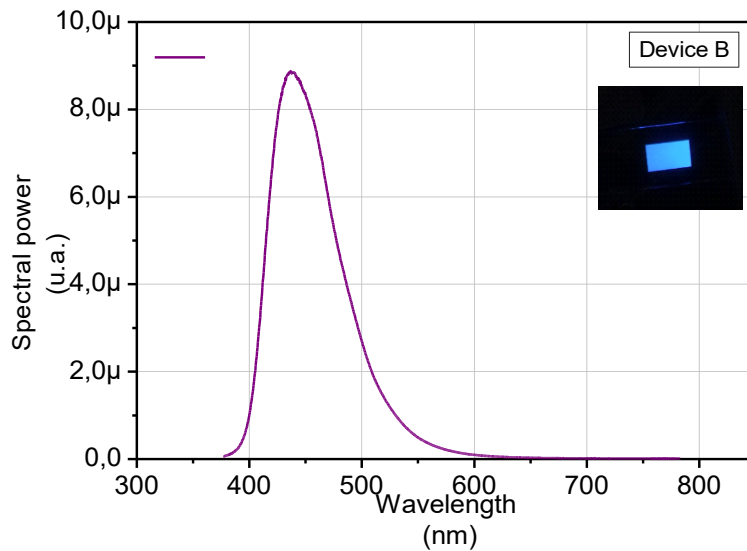


**Figure 6.4** - Spectral power for the Fluorescent device (Device B); in the inset the device under operation

In Figure 6.5 and 6.6, normalized luminance at 40 mA vs. time for the different storage conditions are respectively reported for Device A and B. As it can be seen, all the devices showed degradation during OFF-time period and the observed lifetimes are to be considered too short for OLED applications.

At the other current values, the same normalized luminance curves were obtained, so that luminance efficiency loss was found independent of the applied current over storage time for both types of devices, as shown by the illustrative case in the insets of the Figures 6.5 and 6.6. Moreover, for each current, no operating voltage rise was observed with time.

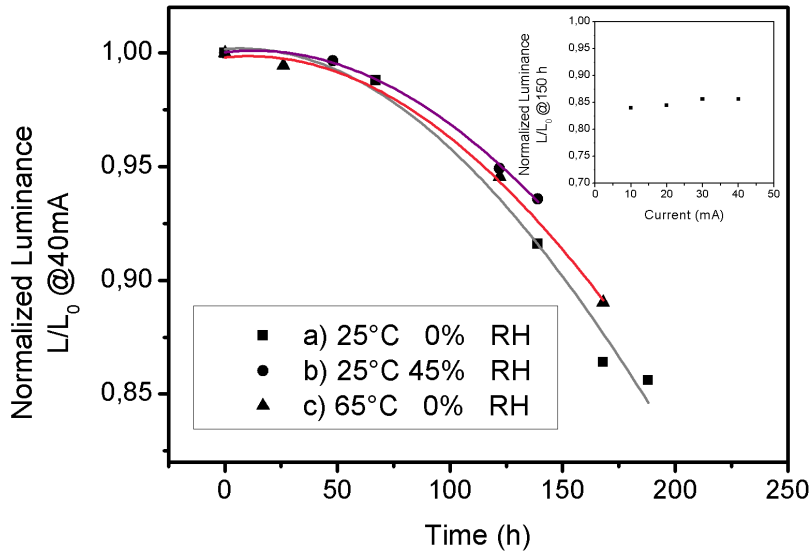


**Figure 6.5** - Normalized luminance at 40 mA for Phosphorescent OLED (Device A) at different storage conditions; in the inset, normalized luminance vs. current is illustrated for a) storage condition.

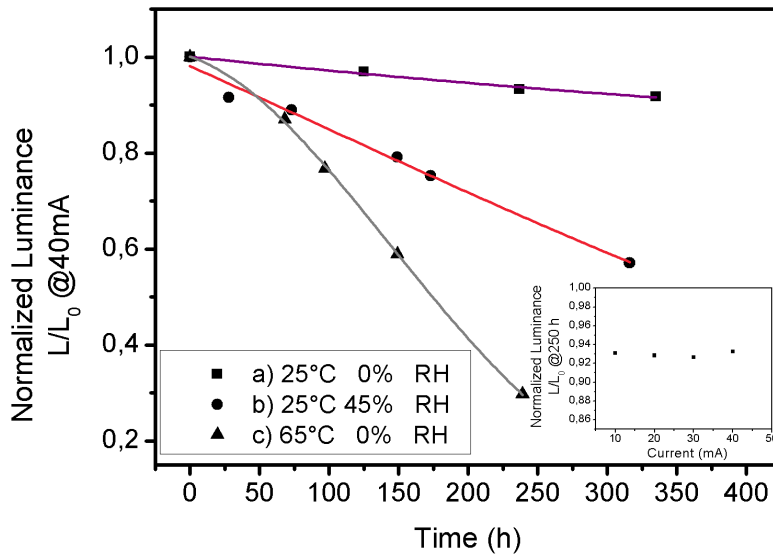


**Figure 6.6.** Normalized luminance at 40 mA for Fluorescent OLED (Device B) at different storage conditions; in the inset, normalized luminance vs. current is illustrated for a) storage condition.

Phosphorescent OLEDs exhibited lower stability than the fluorescent ones (conditions a and b). In addition, their degradation occurred independently from the environmental conditions, pointing out the intrinsic nature of the degradation mechanisms. Considering the low currents used for very short period (some minutes) to measure the luminance, chemical reactions induced by the current can be excluded. Furthermore, because of no variation of the operating voltage, charge mobility remains substantially unchanged. Therefore, such time-dependent luminance appears to be related to physical changes that occur in the bulk properties of the emitting material and affect the exciton radiative recombination rate.

Fluorescent devices proved to be more stable but sensible to the conditioning. Water vapor (condition b) was found to about halve the lifetime of the device, although no dark spots were observed with time, neither a voltage changes at the applied currents: it can be deduced that luminance loss only comes from possible effects of the sorption of the water in the emitting material, so inducing a variation in the molecular arrangement and reducing the ability to emit light. Instead, very strong temperature-dependence of the luminance loss was observed, highlighting once more physical aging process.

Amorphous organic small molecules are not in thermodynamic equilibrium at temperature below their  $T_g$ . In fact, the molecules mobility is not zero in the aging temperature range, typically running from  $T_g$  down to the highest secondary transition  $T_\beta$  (below  $T_\beta$ , segmental motion ceases and the material reaches the truly glass state [60]), and they gradually approach the equilibrium, so that morphological changes occur altering the bulk recombination properties of the material over time. This mechanism, the so called physical aging, is directly related to the relaxation times, mainly influencing the segmental mobility. So, because the luminance monotonically decreases as a function of time, an exponential-based equation was considered for the phenomenological description of the relaxation of the luminance. In particular, data were found to be well fitted using the following distribution of relaxation functions:

$$\frac{L(t)}{L_0} = A e^{-\frac{t}{\tau_1}} e^{-\frac{t^2}{\tau_2}} \quad (5.2)$$

where  $t$ ,  $L_0$ ,  $L(t)$ ,  $A$ ,  $\tau_1$  and  $\tau_2$  are respectively the elapsed time, initial luminance, luminance at time  $t$ , pre-exponential factor and relaxation times.

The presented study has shown therefore the impact of the proposed method. In this specific case the methodology has shed the light on morphological changes in the emitting material induced by physical aging phenomena occurring during shelf OFF time. Therefore, a first consequence of this case study is that the aging range of the emitting layers has to be seriously taken into account for the OLED design and storage. Furthermore combining different experimental method (i.e. electrical stress, storage condition etc) is hence possible to identify single mechanism involved.

## **Chapter 7**

# **7 Conclusion and future perspective**

## **7.1 Conclusion**

In this thesis work has been faced the limited life-time of organic electronic devices especially referred to OLED, that still represents the more critical issue for their broad commercialization. In addition to low stability caused by ambient gases, other degradation phenomena, only recently considered by scientific world, acts to reduce devices lifetime. Multiple factors make this topic difficult to study: on one side the fact that this theme is in its early years but above all the complexity of the involved phenomena (not yet fully identified and understood). In particular, to date, the intrinsic degradation is the most open issue to be solved. Within this work, an innovative methodology for studying organic devices degradation mechanisms has been proposed. This method allows studying separately single phenomena involved in the degradation process. In order to reach this goal resulted very important to separate extrinsic degradation component from the intrinsic one so in this thesis we worked on the following topics:

- reliable evaluation of permeation barriers using the electrical calcium corrosion test
- glass to glass and thin film encapsulation permeation barrier system
- devices (OLED) lifetime under accelerated aging conditions
- intrinsic degradation study: methodology and application

Regarding the first topic a measurement system based on Calcium corrosion test has been first studied, designed and developed taking into account every detail leading to a result alteration such as the series resistance of electrodes shared by current- and voltage contacts, the use of an electrode material which is unable to withstand test conditions, an evaporation sequence probably leading to an enhanced calcium corrosion at the calcium/electrode-border. Consequently, an electrical calcium test layout avoiding these influences has been developed. Then first a glass to glass and later a thin film encapsulation system has been designed and developed in the same way. The Calcium corrosion test measurement system was then used to measure the barrier performances of the developed encapsulation systems revealing values of WVTR in line with literature results obtained through the selected techniques. Particularly had been detected a WVTR value of  $4 \cdot 10^{-6} \text{ g m}^{-2} \text{ day}^{-1}$  and approximately  $10^{-2} \text{ g m}^{-2} \text{ day}^{-1}$  respectively for glass to glass and Thin Film Encapsulation system.

Regarding OLED lifetime, using simple devices, experiments were conducted for one OLED-structure processed on glass. The structure used an ITO bottom contact as well as an aluminum top contact. The realized devices after 3000 hours have lost only a 20% in luminance from the initial value validating the performances of the developed encapsulation solution for devices realized on glass substrate in the same time of observation.

This result if from one side is very encouraging for lifetime issue on the other side is the key element that allows neglecting external effect during further degradation study. The results achieved on these topics results precious to focus on the last aspect faced during this work. In fact using our encapsulation system and applying different experimental techniques, typically not employed, has been possible to put in light single intrinsic degradation mechanism involved. Particularly has been decided to focus on possible phenomena that can occur during OFF-time periods (without electrically stressing the samples). Experiments have been conducted at different storage conditions on two types of blue OLEDs representing the worst stability case. This study revealed , in condition that allow to neglect other degradation source, that physical aging occurs for both types of devices, leading to irreversible time-dependent luminance loss. The proposed method in this case study (accelerated environmental aging

conditions) coupled with other more common used analysis conditions allows to study the degradation topic in a more complete way.

## 7.2 Future perspective

To further improve the results of this work it is possible to work on the different aspects.

Regarding the development of Calcium corrosion test measurement system, it has been taken into account all the issues raised and reported in the literature to date to provide the best reliability and accuracy of the measurement. After all it is possible to suggest some topics for the future:

- the improvement of the calcium test layout and setup to reach a higher sensitivity level
- effort towards a standardization of Calcium test in order to make it not only a WVTR estimation method but a proper measurement system
- investigation on the approximation of the mathematical model including parameters ( $\rho_{Ca}$ ,  $\delta_{Ca}$ ) considered as constant during Calcium corrosion reaction and the assumption of perfectly laterally homogeneous corrosion.

Regarding the barrier technologies, here it has been realized Thin Film sputtered multilayer based on  $Al_2O_3$ . For the future it is possible to work on:

- ALD barriers as it is a promising candidate for high quality thin film encapsulation
- investigation, through variable temperature and humidity measurement, on process quality and defect geometry (macro or nano defects).

Regarding the proposed study methods it could open a variety of new scientific investigation fields on OLED degradation such as:

- stability aimed design using only tested materials (consolidated or new synthesis) and architectures
- development of a complete mathematical model to describe OLED degradation, putting in relation the various mechanism identified
- development of a precise relation between barrier value of WVTR and OLED lifetime.

## 8 Table of Figures

<b>Figure 1.1</b> - Carbon sp <sup>3</sup> hybridization made of three 2p orbitals mixed with 2s orbital forming four hybridized sp <sup>3</sup> states in tetrahedral spatial configuration. Two Carbon sp <sup>3</sup> atoms forming $\sigma$ bond. ....	8
<b>Figure 1.2</b> - Carbon sp <sup>2</sup> hybridization made of two 2p orbitals mixed with 2s orbital forming three hybridized sp <sup>2</sup> states plus one un-hybridized 2p orbital. Two Carbon sp <sup>2</sup> atoms forming double $\sigma$ and $\pi$ bond. ....	8
<b>Figure 1.3</b> - Band structure of a Carbon ring. It can be seen that an energy gap occurs from $\pi$ and $\pi^*$ bands, while bands formed by $\sigma$ and $\sigma^*$ states lie at lower and higher energies (respectively). ....	9
<b>Figure 1.4</b> - Hopping transport mechanism .....	11
<b>Figure 1.5</b> - Hopping conduction: a) nearest neighbor hopping, b) variable range hopping.....	12
<b>Figure 1.6</b> - Schematic of barrier level for Schottky-Richardson thermionic emission.....	15
<b>Figure 1.7</b> - Schematic of barrier level for Fowler-Nordheim tunneling.....	16
<b>Figure 1.8</b> - OTFT in top contact configuration and typical OTFT curves.....	18
<b>Figure 1.9</b> - Four possible configurations for an OTFT. ....	18
<b>Figure 1.10</b> - Schematic of device structures of conventional multi-junction tandem cells.....	19
<b>Figure 1.11</b> - Schematic of device structures of (a) conventional single-junction cell, (b) inverted single-junction cell [2].....	20
<b>Figure 1.12</b> - Schematic of a bottom up OLED structures.....	21
<b>Figure 1.13</b> - General multi-layer sequence for small molecules OLEDs.....	22
<b>Figure 1.14</b> - Dark spot formation.....	24
<b>Figure 2.1</b> - Schematic of the permeation process.....	28
<b>Figure 2.2</b> - Typical isotherm plots of sorbed concentration versus ambient vapour pressure: (I) Henry's law; (II) Langmuir equation; (III) Flory-Huggins equation; (IV) BET equation [12]. ....	29
<b>Figure 2.3</b> - Typical permeation curve: amount of permeated penetrant Q, as a function of time, t. ....	32

<b>Figure 2.4</b> - Principle of water vapor permeation measurement using a carrier gas method such as a coulometric device [9].	34
<b>Figure 2.5</b> - Setup for mass spectrometric permeation measurement [9].	35
<b>Figure 2.6</b> - Different calcium test setups. The conversion of calcium (Ca) can be monitored by optical transmission (left and center) or by electrical resistance measurements (right). For both principles, two variants are possible: placing the Ca layer directly on the barrier (left) causes local Ca conversion at barrier pinholes and thereby allows the characterization of pinhole sizes and densities. Placing the calcium layer with a connecting gas volume causes evenly distributed Ca consumption (center and right) [9].	37
<b>Figure 2.7</b> - Requirements in terms of WVTR (x axis) and (y axis) for various commercial areas	38
<b>Figure 2.8</b> - Schematic of a glass to glass encapsulation system with getter added within the volume	40
<b>Figure 2.9</b> - Schematic of an encapsulation system with barrier layer laminated on the device surface	41
<b>Figure 2.10</b> - Schematic of an encapsulation system realized with the Thin Film approach	42
<b>Figure 2.11</b> - Various steps of one ALD cycle for the deposition of an Al <sub>2</sub> O <sub>3</sub> monolayer [9].	44
<b>Figure 2.12</b> - Classification of defects [38]: permeation of water and oxygen through barrier layers is dominated by nano- and macro-defects. Lattice interstices are too small for both of them.	46
<b>Figure 2.13</b> - Most used models employed to explain permeation through single thin films on polymer substrates [9]. In all models, except for the Ideal-Laminate model, permeation occurs solely through pinholes with the barrier acting as an inert block.	47
<b>Figure 2.14</b> - Tortuous path model: thanks to smooth polymer interlayers, defects of successive layers are spatially separated. The longer distance lowers the speed of diffusion and increases the lag time [10].	48
<b>Figure 2.15</b> - Schematic illustration of the effective diffusional thickness $l$ of the polymer layer. This results in a path length which is much longer than the polymer physical thickness $d_p$ [10]	49
<b>Figure 3.1</b> - The gas volume allows water vapor to distribute and shall ensure for homogeneous corrosion.	54

<b>Figure 3.2</b> - Schematic of the designed layout for electrical corrosion Calcium test measurement system .....	54
<b>Figure 3.3</b> - Keithley2400 SourceMeter a) and the control software developed for the automatic measure .....	55
<b>Figure 3.4</b> - Votsch climate chamber utilized for Electrical Calcium Test conditionings and measurement station for accommodation of the sample.....	56
<b>Figure 3.5</b> - Kurt J. Lesker Company evaporator system incorporated in a Jacomex glove box used for metal evaporations.....	56
<b>Figure 3.6</b> - Nordson EFD automatic dispenser used for resin dispensation included in an MBRAUN glove box.....	57
<b>Figure 3.7</b> - Conductance curve versus time for encapsulated 100 nm thick Ca pad measured at 25°C and 90%RH.....	59
<b>Figure 4.1</b> - OLEDs encapsulation layouts with rectangular emitting area of 1 cm <sup>2</sup> while the glass lid used for the encapsulation.....	63
<b>Figure 4.2</b> - OLEDs encapsulation layouts studied for the encapsulation of three devices with 0.07 cm <sup>2</sup> round area simultaneously.....	63
<b>Figure 4.3</b> - On the left the glue dispensation through Nordson EFD dispenser while on the right the glass lid positioning.....	64
<b>Figure 4.4</b> - Encapsulated sample with a optimized coverage of the lid frame.....	65
<b>Figure 4.5</b> - The UV curing process realized with an optic fiber connected to the UV lamp. ....	66
<b>Figure 4.6</b> - Sample realized for the characterization through Electrical Calcium Test of glass to glass encapsulation system.....	67
<b>Figure 4.7</b> - Schematic of a glass to glass encapsulation system with a getter into the sealed volume .....	67
<b>Figure 4.8</b> - Thin adhesive getter Dryflex produced by SAES Getter .....	68
<b>Figure 4.9</b> - Conductance versus time curves for a Calcium sample without getter in the sealed volume.....	69
<b>Figure 4.10</b> - Conductance versus time curves for a Calcium sample with getter in the sealed volume.....	69
<b>Figure 4.11</b> - OLEDs layout used for the validation samples. Dashed line identifies the cross section.....	71
<b>Figure 4.12</b> - Structure and energy levels for the device with Alq <sub>3</sub> as emitter layer.....	71
<b>Figure 4.13</b> - Schematic of the structure of the encapsulated device	72

<b>Figure 4.14</b> - Spectral power of the realized devices. In the inset it has been reported one of the devices under operation.....	72
<b>Figure 4.15</b> - Luminance vs time curve @ 40 mA cm <sup>-2</sup> for the device without getter.....	73
<b>Figure 4.16</b> - Luminance vs time curve @ 40 mA cm <sup>-2</sup> for the device with getter.....	73
<b>Figure 5.1</b> - Plasma discharge in Argon in the Kurt J. Lesker sputtering system used for RF sputtering deposition of Al <sub>2</sub> O <sub>3</sub> . ....	77
<b>Figure 5.2</b> - PermeoH <sub>2</sub> O permeabilimeter by ExtraSolution for WVTR barrier film measurement. ....	78
<b>Figure 5.3</b> - WVTRs @ 50°C and 90%RH of PEN with Al <sub>2</sub> O <sub>3</sub> at fixed thickness (120 nm) deposited with different Ar flow. ....	79
<b>Figure 5.4</b> - WVTRs @ 38°C and 90%RH of PEN samples coated with Al <sub>2</sub> O <sub>3</sub> of different thicknesses.....	79
<b>Figure 5.5</b> - Morphological surface of PEN samples printed with: a) organic coating diluted with 50wt% of solvent; b) organic coating diluted with 100wt% of solvent; c) organic coating diluted with 100wt% of solvent + solvent post-treatment; d) organic coating diluted with 150wt% of solvent + slow drying (1h in Petri).....	82
<b>Figure 5.6</b> - Schematic of realized multilayer barrier structure. ....	83
<b>Figure 5.7</b> - UV-VIS-NIR transmittance measurements of multilayer barrier structure on PEN substrate with different number of dyads (pair of layers of Al <sub>2</sub> O <sub>3</sub> -organic).....	84
<b>Figure 5.8</b> - Sample on PEN realized for the evaluation through Electrical Calcium Test of multilayer barrier structure.....	84
<b>Figure 5.9</b> - Conductance curves versus time (from electrical Ca test) at 38°C and 90%RH of multilayer barrier structure on PEN substrate with different number of dyads (pair of layers of Al <sub>2</sub> O <sub>3</sub> -organic)....	85
<b>Figure 6.1</b> - Structure and energy levels for the Phosphorescent device (Device A).....	90
<b>Figure 6.2</b> - Structure and energy levels for the Fluorescent device (Device B).....	90
<b>Figure 6.3</b> - Structure and energy levels for the Phosphorescent device (Device A); in the inset the device under operation.....	91
<b>Figure 6.4</b> - Spectral power for the Fluorescent device (Device B); in the inset the device under operation.....	92
<b>Figure 6.5</b> - Normalized luminance at 40 mA for Phosphorescent OLED (Device A) at different storage conditions; in the inset,	

normalized luminance vs. current is illustrated for a) storage  
condition..... 93

## 9 Bibliography

- [1] O. J. Weiss, R. Krause and R. Paetzold., "Organic Thin Film Devices for Displays and Lighting," *Advances in Solid State Physics*, vol. 46, pp. 321-332, 2008.
- [2] M. D. Fayer, "Elements of Quantum Mechanics," New York, Oxford University Press, 2001, pp. 158-162.
- [3] S. M. Sze, *Semiconductor Physics and Devices*, Second Edition, Wiley, 1981.
- [4] Y.-W. Su, S.-C. Lan and K.-H. Wei, "Organic photovoltaics," *Materials Today*, vol. 15, pp. 554-562, 2012.
- [5] W. Shockley and H. J. Queisser, "Detailed Balance Limit of Efficiency of p-n Junction Solar Cells," *Journal of Applied Physics*, vol. 32, pp. 510-519, 1961.
- [6] C. W. Tang and S. A. VanSlyke, "Organic electroluminescent diodes 51(12), 913-15.," *Applied Physics Letters*, vol. 51, pp. 913-915, 1987.
- [7] S. Reineke, M. Thomschke, B. Lüssem and K. Leo, "White organic light-emitting diodes: Status and perspective," *Rev. Mod. Phys.*, vol. 85, p. 1245, 2013.
- [8] H. Aziz and Z. D. Popovic, "Degradation Phenomena in Small-Molecule Organic Light-Emitting Devices," *Chemical Materials*, vol. 16, p. 4522-4532, 2004.
- [9] F. So and D. Kondakov, "Degradation Mechanisms in Small-Molecule and Polymer Organic Light-Emitting Diodes," *Advanced Materials*, vol. 22, p. 3762-3777, 2010.
- [10] P. E. Burrows, V. Bulovic, S. R. Forrest, L. S. Sapochak, D. M. McCarty and M. E. Thompson, "Reliability and degradation of organic light emitting devices," *Applied Physics Letters*, vol. 65, pp. 2922-2924, 1994.
- [11] Z. D. Popovic and H. Aziz, "Reliability and Degradation Phenomena in Small-Molecule Organic Light-Emitting Devices," *IEEE Journal on Selected Topics in Quantum Electronics*, vol. 8, pp. 362-371, 2002.
- [12] S. Lim, W. Wang and S. Chua, "Understanding Dark Spot Formation and Growth in OLEDs by Controlling Pinhole Size

and Shape," *Advanced Functional Materials*, vol. 12, p. 513–518, 2002.

- [13] L. Muller-Meskamp, J. Fahlteich and F. C. Krebs, "Barrier Technology and Applications," in *Stability and Degradation of Organic*, John Wiley & Sons, 2012, pp. 269-329.
- [14] G. L. Graff, R. E. Williford and P. E. Burrows, "Mechanisms of vapor permeation through multilayer barrier films: Lag time versus equilibrium permeation.," *Journal of Applied Physics*, vol. 96, p. 1840, 2004.
- [15] S. Brunauer, P. H. Emmett and E. Teller, "Adsorption of Gases in Multimolecular Layers," *Journal of the American Chemical Society*, Vols. 60., p. 309–319, 1938.
- [16] C. E. Rogers, "Chapter 6," in *Physics and Chemistry of the Organic Solid State. Volume 2*, New York, Interscience, 1965.
- [17] J. COMYN, *Polymer Permeability*, London: Chapman & Hall, 1985.
- [18] J. R. F. S. A. Stern, "Permeability of Polymers to Gases and Vapors," in *Physical Properties of Polymers Handbook*, New York, Springer , 2007, pp. 1033-1047.
- [19] R. M. Barrer, *Diffusion in and Through Solids*, Cambridge: Cambridge University Press, 1951.
- [20] C. Rogers, "Permeation of Gases and Vapours in Polymers," in *Polymer Permeability*, Springer, 1985, pp. 11-73.
- [21] P. Burrows, G. Graff, M. Gross, P. Martin, M. Shi, M. Hall, E. Mast, C. Bonham, W. Bennett and M. Sullivan, "Ultra barrier flexible substrates for flat panel displays," *Displays*, vol. 22, no. 2, pp. 65-69, 2001.
- [22] A. Ranade, N. A. D'Souza, R. M. Wallace and B. E. Gnade, "High sensitivity gas permeability measurement system for thin plastic films," *Rev. Sci. Instrum.* , vol. 76, 2005.
- [23] H. Norenberg, G. D. W. Smith, G. A. D. Briggs, T. Miyamoto and T. Tsukahara, "A New Method for Measuring Low Levels of Water Vapor Permeation Through Polymers and Permeation Barrier Coatings," in *45th Annual Technical Conference of the Society of Vacuum Coaters*, 2002.
- [24] P. J. Brewer, B. A. Goody, Y. Kumar and M. J. T. Milton,

- "Accurate measurements of water vapor transmission through high-performance barrier layers," *Rev. Sci. Instrum.*, vol. 83, 2012.
- [25] S. Cros, M. Firon, S. Lenfant, P. Trouslard and L. Beck, "Study of thin calcium electrode degradation by ion beam analysis," *Nuclear Instruments and Methods in Physics Research Section B: Beam Interactions with Materials and Atoms*, vol. 251, pp. 257-260, 2006.
- [26] H. J. Svec and C. Apel, "Kinetics of the Reaction Between Calcium and Water Vapor," *Journal of the Electrochemical Society*, vol. 104, pp. 346-349., 1957.
- [27] J. S. J. Gregg and W. B. Jepson, "The oxidation of calcium in moist oxygen," *Journal of the Chemical Society*, vol. 0, pp. 884-888, 1961.
- [28] J. H. Choi, Y. M. Kim, Y. W. Park, J. W. Huh, B. K. Ju, I. S. Kim and H. N. Hwang, "Evaluation of gas permeation barrier properties using electrical measurements of calcium degradation," *Review of Scientific Instruments*, vol. 78, no. 6, 2007.
- [29] S. Schubert, H. Klumbies, L. Müller-Meskamp and K. Leo, "Electrical calcium test for moisture barrier evaluation for organic devices," *Rev. Sci. Instrum.*, vol. 82, 2011.
- [30] J. S. Lewis and M. S. Weaver, "Thin-Film Permeation-Barrier Technology for Flexible Organic Light-Emitting Devices," *IEEE Journal of Selected Topics in Quantum Electronics*, vol. 10, pp. 45-57, 2004.
- [31] B. Henry, H. E. Assender, A. G. Erlat, C. R. M. Grovenor, G. A. D. Briggs, T. Miyamoto and Y. Tsukahara, "Gas Barrier Properties of Transparent Metal Oxide Coatings on PET Film," in *Proceedings of the 47th Annual Technical Conference of the Society of Vacuum*, 2004.
- [32] C. Charton, N. Schiller, M. Fahland, A. Hollander, A. Wedel and K. Noller, "Development of high barrier films on flexible polymer substrates," *Thin Solid Films*, vol. 502, pp. 99-103, 2006.
- [33] M. Fahland, T. Vogt, B. Meyer, J. Fahlteich, N. Schiller, M. Vinnichenko and F. Munnik, "Deposition of functional coatings on polyethylene terephthalate films by magnetron-plasma-

enhanced chemical vapor deposition," *Thin Solid Films*, vol. 517, p. 3043–3047, 2009.

- [34] C. Charton, M. Fahland and N. Schiller, "Plasma Enhanced CVD Process Using a Dual Magnetron as Plasma Source," in *Proceedings of the 48th Annual Technical Conference of the Society of Vacuum Coaters*, 2005.
- [35] R. Nyderle, M. Fahland, R. Bluthner, J. Fahlteich and S. Bunk, "Recent Developments with Magnetron PECVD for Industrial Applications," in *Proceedings of the 53rd Annual Technical Conference of the Society of Vacuum Coaters*, 2010.
- [36] P. F. Carcia, R. S. McLean, M. D. Groner, A. A. Dameron and S. M. George, "Gas diffusion ultrabarrriers on polymer substrates using Al<sub>2</sub>O<sub>3</sub> atomic layer deposition and SiN plasma-enhanced chemical vapor deposition," *Journal of Applied Physics*, vol. 106, 2009.
- [37] S. M. George, A. W. Ott and J. W. Klaus, "Surface Chemistry for Atomic Layer Growth," *The Journal of Physical Chemistry*, vol. 100, no. 31, p. 13121–13131, 1996.
- [38] A. Dameron, S. Davidson, B. Burton, P. Carcia, R. McLean and S. M. George, "Gas Diffusion Barriers on Polymers Using Multilayers Fabricated by Al<sub>2</sub>O<sub>3</sub> and Rapid SiO<sub>2</sub> Atomic Layer Deposition," *The Journal of Physical Chemistry C*, vol. 112, p. 4573–4580.
- [39] W. Decker and B. M. Henry, "Basic Principles of Thin Barrier Coatings," in *Proceedings of the 45th Annual Technical Conference of the Society of Vacuum Coaters*, 2002.
- [40] L. Moro and R. J. Visser, "Barrier Films for Photovoltaics Applications," in *Organic Photovoltaics: Materials, Device Physics, and Manufacturing Technologies*, Weinheim, WILEY-VCH Verlag GmbH & Co., 2008, p. 491–510.
- [41] Y. G. Tropsha and N. G. Harvey, "Activated Rate Theory Treatment of Oxygen and Water Transport through Silicon Oxide/Poly(ethylene terephthalate) Composite Barrier Structures," *Journal of Physical Chemistry B*, vol. 5647, p. 2259–2266, 1997.
- [42] A. Roberts, B. Henry, A. Sutton, C. Grovenor, G. Briggs, T. Miyamoto, M. Kano, Y. Tsukahara and M. Yanaka, "Gas

- permeation in silicon-oxide/polymer (SiO<sub>x</sub>/PET) barrier films: role of the oxide lattice, nano-defects and macro-defects," *Journal of Membrane Science*, vol. 208, p. 75–88, 2002.
- [43] W. Prins and J. J. Hermans, "Theory of Permeation Through Metal Coated Polymer Films," *The Journal of Physical Chemistry*, vol. 63, no. 5, p. 716–719, 1959.
- [44] M. Hanika, H.-C. Langowski, U. Moosheimer and W. Peukert, "Inorganic Layers on Polymeric Films – Influence of Defects and Morphology on Barrier Properties," *Chemical Engineering and Technology*, vol. 26, pp. 605-614, 2003.
- [45] Y. Leterrier, "Durability of nanosized oxygen-barrier coatings on polymers – Internal stresses," *Progress in Material Science*, vol. 48, no. 1, 2003.
- [46] J. H. Choi, Y. M. Kim, Y. W. Park, B. K. Ju, I. S. Kim and H. N. Hwang, "Permeation-Rate Measurements System and Its Application to Polymeric Substrates," *Symposium Digest of Technical Papers*, vol. 39, no. 1, p. 1485–1487, 2008.
- [47] G. Nisato, P. Bouten and P. Slikkerveer, "Evaluating high performance diffusion barriers: the calcium test," in *Asia Display Proceedings*, 2001.
- [48] L. M.-M. H. Klumbies, T. Mönch, S. Schubert and K. Leo, "The Influence Of Laterally Inhomogeneous Corrosion On Electrical And Optical Calcium Moisture Barrier Characterization," *Review Of Scientific Instruments*, vol. 84, pp. 1-8, 2013.
- [49] R. Paetzold, A. Winnacker, D. Henseler, V. Cesari and K. Heuser, "Permeation rate measurements by electrical analysis of calcium corrosion," *Review of Scientific Instruments*, vol. 74, pp. 5147-5150, 2003.
- [50] G. Nisato, "Permeation Measurements Using The Calcium-Test," White Paper For The Use Of OE-A Members, 2013.
- [51] R. M. O., D. A. A. and K. M. D., "Quantitative calcium resistivity based method for accurate and scalable water vapor transmission rate measurement," *Review of Scientific Instruments*, vol. 82, no. 8, 2011.
- [52] J.-S. Park, H. Chae, H. K. Chung and S. I. Lee, "Thin film encapsulation for flexible AM-OLED: a review," *Semiconductor*

*science and technology*, vol. 26, no. 3, 2011.

- [53] H.-M. Kim, K. Bae, S.-B. Seo, S. Sohn and D. Kim, "Homogeneous Al<sub>2</sub>O<sub>3</sub> Multilayered Films Deposited on Poly(ethylene terephthalate) by Facing-Target Sputtering System for Thin-Film Passivation of Organic Light-Emitting Diodes," *Japanese Journal of Applied Physics*, vol. 52, 2013.
- [54] Y.-H. Choi, Y. G. Lee, X. Bulliard, K.-H. Lee, S. Lee, D. Choi, J.-J. Park and J. M. Kim, "Homogeneous Al<sub>2</sub>O<sub>3</sub> multilayer structures with reinforced mechanical stability for high-performance and high-throughput thin-film encapsulation," *Scripta Materialia*, vol. 62, no. 7, pp. 447-450, 2010.
- [55] S. Cros, R. de Bettignies, S. Berson, S. Bailly, P. Maise, N. Lemaitre and S. Guillerez, *Solar Energy Materials & Solar Cells*, vol. 95, p. S65–S69, 2011.
- [56] P. Dupuis, A. Alchaddoud, L. Canale and G. Zissis, "OLED aging signature characterization under combined thermal and electrical stresses," in *Conference Proceedings of ISEIM*, 2014.
- [57] I. R. d. Moraes, S. Scholz, B. Lussem and K. Leo, "Analysis of chemical degradation mechanism within sky blue phosphorescent organic light emitting diodes by laser-desorption/ionization time-of-flight mass spectrometry," *Organic Electronics*, vol. 12, pp. 341-347, 2011.
- [58] R. Seifert, I. R. d. Moraes, S. Scholz, M. C. Gather, B. Lussem and K. Leo, "Chemical degradation mechanism of highly efficient blue phosphorescent emitters used for organic light emitting diodes," *Organic Electronics*, vol. 14, pp. 115-123, 2013.
- [59] E. Santoro, S. Aprano, G. Sico, M. R. Fiorillo, M. Maglione, P. Tassini, A. Rubino and C. Minarini, "Evaluation of the stability of different encapsulated blue oleds," in *Fotonica AEIT Italian Conference on Photonics Technologies*, Torino, 2015.
- [60] L. C. E. Struik, "Physical Aging in Plastics and Other Glassy Materials," *Polymer Engineering and Science*, vol. 17, pp. 165-173, 1977.